RESEARCH ARTICLE SUMMARY

CELL ENGINEERING

Programming tissue-sensing T cells that deliver therapies to the brain

Milos S. Simic†, Payal B. Watchmaker†, Sasha Gupta, Yuan Wang, Sharon A. Sagan, Jason Duecker, Chanelle Shepherd, David Diebold, Psalm Pineo-Cavanaugh, Jeffrey Haegelin, Robert Zhu, Ben Ng, Wei Yu, Yurie Tonai, Lia Cardarelli, Nishith R. Reddy, Sachdev S. Sidhu, Olga Troyanskaya, Stephen L. Hauser, Michael R. Wilson, Scott S. Zamvil*, Hideho Okada*, Wendell A. Lim*

INTRODUCTION: Treatment of central nervous system (CNS) disorders such as brain tumors, neuroinflammation, and neurodegeneration remains challenging because it is difficult to effectively deliver molecular therapeutics to the brain. Moreover, it is difficult to restrict the action of these therapeutics to the brain to avoid peripheral or systemic toxicities.

RATIONALE: Immune cells have evolved to infiltrate diverse tissues, integrate information about their surroundings, and reshape tissue ecosystems. T cells, for example, can cross the blood–brain barrier under healthy and pathogenic conditions. These properties make them ideal delivery vehicles for the CNS. In principle, if we program cells to selectively and autonomously deliver therapeutic payloads to the brain, then we could reduce systemic off-target toxicity and increase efficacy. We hypothesized that it might be possible to engineer immune cells to act only in a tissue-specific manner. One way to harness T cells to deliver payloads selectively to the brain would be to engineer them to recognize normal (nondisease) CNS-specific antigens and to use this anatomical cue to locally induce the production of a therapeutic agent. This cell-based CNS-specific delivery system could serve as a general platform for treating diverse CNS diseases.

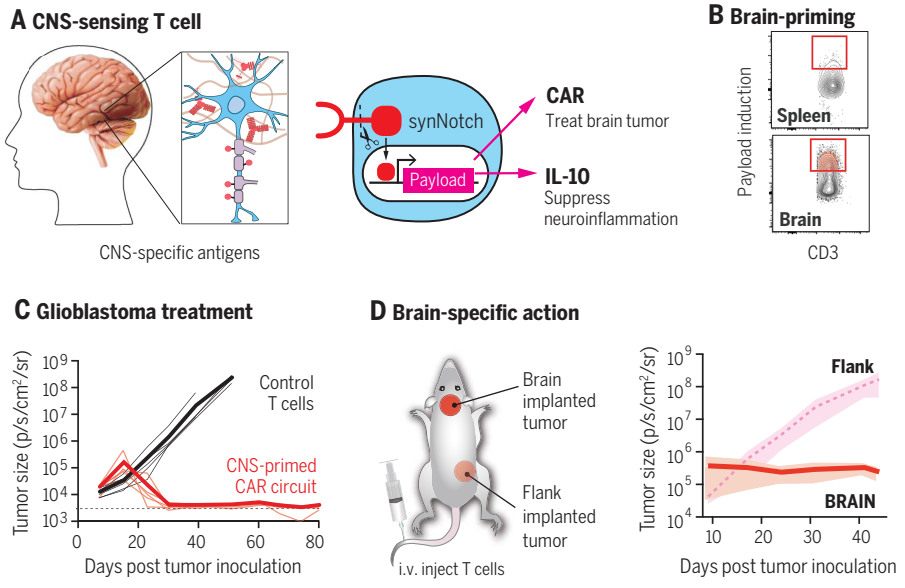

Programming tissue-sensing T cells to deliver therapeutics to the brain. (**A**) We designed T cells that can recognize normal endogenous CNS-specific antigens using a synNotch receptor to induce the production of therapeutic payloads specifically in the brain. For example, induction of a chimeric antigen receptor (CAR) could be used to target brain tumors, or induction of an anti-inflammatory cytokine such as IL-10 could be used to suppress neuroinflammation. This CNS-specific delivery system could be a general platform for treating diverse CNS diseases without the risk of systemic toxicity. (**B**) When injected in a mouse, CNS-sensing T cells specifically expressed the synNotch-induced payload in the brain, but not in the periphery (spleen). (**C**) In a glioblastoma mouse model, CNS-sensing T cells equipped to express an anti–ephrin type A receptor 2/IL-13 receptor α2 (EphA2/IL13Rα2) CAR efficiently and durably cleared the brain tumors. (**D**) In a two-tumor model, the CNS-sensing T cells only cleared the brain-implanted tumor (solid red line), but not a flank-implanted tumor expressing the identical CAR target antigens (dotted pink line). Therefore, the T cells are selectively primed only in the brain.

RESULTS: We created a set of brain-sensing T cells programmed to locally deliver therapeutic payloads customized for cancer or neuroinflammation. First, we identified a set of CNS-specific extracellular ligands using publicly available expression data to establish potential brain "GPS" markers. We identified proteins such as brevican (BCAN), which are components of the brain's highly unique extracellular matrix and might be exploited for tissue-specific recognition. We screened for antibodies against these CNS-specific antigens and used them to build CNS-activated synthetic Notch (synNotch) receptors, engineered receptors that sense an extracellular antigen and respond by inducing a transcriptional response.

To demonstrate the therapeutic potential of this approach, we used this platform to locally induce a set of genetically encoded payloads directed toward different CNS diseases. Brain-sensing T cells that induced CAR expression were able to treat primary and secondary brain cancers, including mouse models of glioblastoma and breast cancer metastases, without off-target attack of tissues outside of the brain. Conversely, CNS-induced expression of the immunosuppressive cytokine interleukin-10 (IL-10) ameliorated neuroinflammation in experimental autoimmune encephalomyelitis, a mouse model of multiple sclerosis.

CONCLUSION: This tissue-targeted cell induction strategy provides two levels of specificity. First, the cell shows anatomically restricted specificity, as cells are only induced in the CNS, and second, the payload (e.g., CAR, cytokine, antibody) has its own intrinsic molecular targeting specificity. This nested, multiscale targeting strategy mimics the principles of natural biological specificity, avoiding potential unwanted systemic cross-reactions of the molecular payload while focusing its actions more effectively on the target tissue. These results suggest that brain-sensing cells could be used as a general platform to treat a broader set of CNS diseases, including brain tumors, brain metastases, neuroinflammation, and neurodegeneration. Although we focused here on targeting the CNS, this concept could be applied to a broader set of tissues. Tissue-targeted therapeutic cells provide an approach to integrating endogenous and disease signals to generate therapies that are more specific and effective. ■

The list of author affiliations is available in the full article online.
*Corresponding author. Email: zamvil@ucsf.neuroimmunol.org (S.S.Z.); hideho.okada@ucsf.edu (H.O.); wendell.lim@ucsf.edu (W.A.L.)
†These authors contributed equally to this work.
Cite this article as M. S. Simic *et al.*, *Science* **386**, eadl4237 (2024). DOI: 10.1126/science.adl4237

READ THE FULL ARTICLE AT
https://doi.org/10.1126/science.adl4237

RESEARCH ARTICLE

CELL ENGINEERING

Programming tissue-sensing T cells that deliver therapies to the brain

Milos S. Simic[1]†, Payal B. Watchmaker[2]†, Sasha Gupta[3], Yuan Wang[4,5], Sharon A. Sagan[3], Jason Duecker[1], Chanelle Shepherd[1], David Diebold[2], Psalm Pineo-Cavanaugh[2], Jeffrey Haegelin[2], Robert Zhu[1], Ben Ng[1], Wei Yu[1], Yurie Tonai[1], Lia Cardarelli[6], Nishith R. Reddy[1], Sachdev S. Sidhu[6], Olga Troyanskaya[4,5,7], Stephen L. Hauser[3], Michael R. Wilson[3], Scott S. Zamvil[3,8]*, Hideho Okada[2,9,10]*, Wendell A. Lim[1,9]*

To engineer cells that can specifically target the central nervous system (CNS), we identified extracellular CNS-specific antigens, including components of the CNS extracellular matrix and surface molecules expressed on neurons or glial cells. Synthetic Notch receptors engineered to detect these antigens were used to program T cells to induce the expression of diverse payloads only in the brain. CNS-targeted T cells that induced chimeric antigen receptor expression efficiently cleared primary and secondary brain tumors without harming cross-reactive cells outside of the brain. Conversely, CNS-targeted cells that locally delivered the immunosuppressive cytokine interleukin-10 ameliorated symptoms in a mouse model of neuroinflammation. Tissue-sensing cells represent a strategy for addressing diverse disorders in an anatomically targeted manner.

Most drugs act systemically, and even if they have strong specificity for their molecular target, they can show toxicities because most targets are expressed in both diseased and normal tissues. Ideally, we would like to restrict the activity of these drugs only to specific, disease-relevant tissues. Targeting central nervous system (CNS) disorders such as brain tumors, neuroinflammation, and neurodegeneration is a particularly challenging example (*1*). Achieving efficacy and minimizing toxicity is very difficult because of the barriers to delivering molecular therapeutics to the brain and because drug targets can often also be expressed in tissues outside of the brain (*2*).

Cell therapies potentially provide a solution to this conundrum because it may be possible to engineer a cell to act only in a tissue-specific manner. For example, using a cell to selectively and autonomously deliver therapeutic payloads to the brain could reduce systemic off-target toxicity and also increase efficacy. Immune cells have evolved to infiltrate diverse tissues, respond to injury or infection, and reshape tissue ecosystems, all properties that may make them suitable to act as local therapeutic delivery vehicles. T cells can cross the blood–brain barrier (BBB) under both healthy and pathogenic conditions (*3*). One way to harness T cells to deliver payloads selectively to the brain would be to engineer them to recognize normal (nondisease) CNS-specific antigens and then use these to trigger the production of a therapeutic agent. Such a cell-based, CNS-specific delivery system could serve as a common platform to treat diverse types of CNS diseases.

We created a set of programmable brain-sensing T cells engineered to locally deliver therapeutic payloads customized for cancer or neuroinflammation. We identified a set of CNS-specific extracellular ligands, screened for antibodies against these, and used them to generate CNS-activated synthetic Notch (synNotch) receptors (engineered receptors that sense an extracellular antigen and respond by inducing a transcriptional response) (*4*). As a proof-of-principle, we harnessed this platform to locally produce a set of genetically encoded payloads directed toward different CNS diseases. CNS-triggered expression of chimeric antigen receptors (CARs) was used to treat primary and secondary brain cancers, including mouse models of glioblastoma and breast cancer metastases. Conversely, CNS-induced expression of the immunosuppressive cytokine interleukin-10 (IL-10) ameliorated neuroinflammation in experimental autoimmune encephalomyelitis (EAE), a mouse model of multiple sclerosis (MS). This tissue-targeted cell strategy provides dual-level targeting specificity: Production of the therapeutic payload is anatomically restricted only to the tissue of interest (here, the CNS), and the payload itself also has its own intrinsic molecular targeting specificity within the target tissue. Such a local delivery strategy thereby avoids potential toxic systemic cross-reactions of the molecular payload in other nondisease tissues.

Bioinformatic screening for CNS-specific recognition antigens

Myelin oligodendrocyte glycoprotein (MOG), a surface molecule on myelinating oligodendrocytes, can be used to help target brain cancers (*5*). In diseases involving demyelination and neuroinflammation, however, molecules such as MOG are likely to be disrupted. Therefore, we wanted to systematically identify and evaluate a broader range of candidate brain-specific antigens. We performed a comprehensive bioinformatic search for brain-specific surface or extracellular molecular features that might be used for specific delivery to the brain (Fig. 1A). Ideal target antigens should be expressed only within the CNS and not in other tissues. Such an antigen should also be expressed throughout the brain in large amounts. To identify antigens that fit these criteria, we used a pipeline of bioinformatic filters (fig. S1A). We used the publicly available Genotype Tissue Expression project (GTEx) RNA-sequencing (RNA-seq) data from healthy tissues to establish a list of the top 500 brain-specific extracellular antigens using a weighted clustering-based score that selected for maximum separation of RNA abundance in the brain relative to that in other tissues (*6*). We further narrowed our list down to 59 candidate extracellular antigens using the Human Protein Atlas (HPA) to confirm protein expression (versus RNA) and expression throughout the brain (fig. S1B). This analysis identified candidate extracellular molecules that are expressed both specifically and in large amounts throughout the brain. A gene ontology (GO) term analysis for cellular components of the 59 candidates further confirmed their CNS and anatomical location enrichment (fig. S1C).

CNS extracellular matrix proteins and surface proteins on neurons and glial cells are highly brain specific

The top two candidate genes to emerge from this analysis, chondroitin sulfate proteoglycan 5 (CSPG5) and brevican (BCAN), are part of the CNS extracellular matrix (ECM). The brain has a distinct ECM composition that includes perineural net structures that stabilize synapses and surround neural cell bodies (*7*). These structures are composed of tenascin R and hyaluronan, which are associated with a family

[1]UCSF Cell Design Institute and Department of Cellular & Molecular Pharmacology, University of California San Francisco, San Francisco, CA, USA. [2]Department of Neurological Surgery, University of California San Francisco, San Francisco, CA, USA. [3]Weill Institute for Neurosciences, Department of Neurology, University of California San Francisco, San Francisco, CA, USA. [4]Department of Computer Science, Princeton University, Princeton, NJ, USA. [5]Lewis-Sigler Institute of Integrative Genomics, Princeton University, Princeton, NJ, USA. [6]School of Pharmacy, University of Waterloo, Waterloo, Ontario, Canada. [7]Center for Computational Biology, Flatiron Institute, New York, NY, USA. [8]Program in Immunology, University of California San Francisco, San Francisco, CA, USA. [9]Parker Institute for Cancer Immunotherapy, San Francisco, CA, USA. [10]Helen Diller Cancer Center, University of California San Francisco, San Francisco, CA, USA.
*Corresponding author. Email: zamvil@ucsf.neuroimmunol.org (S.S.Z.); hideho.okada@ucsf.edu (H.O.); wendell.lim@ucsf.edu (W.A.L.)
†These authors contributed equally to this work.

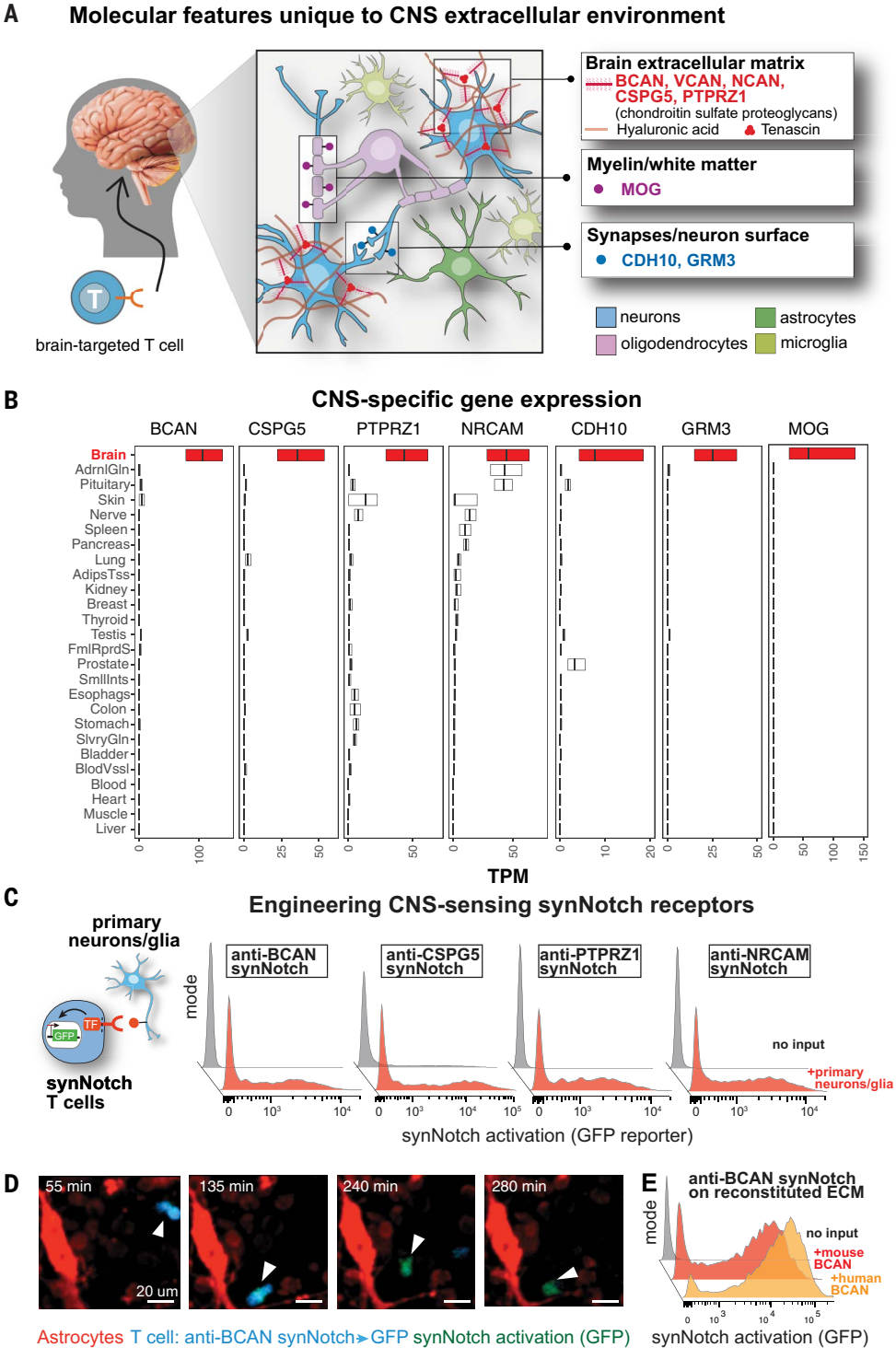

Fig. 1. Identification of CNS-specific extracellular antigens that can be recognized by synNotch receptors. (**A**) Conceptual rationale for the design of therapeutic T cells that can recognize CNS-specific antigens to trigger a therapeutic response locally. Specific extracellular molecular features of the CNS that could be used for recognition are highlighted. (**B**) Box plots showing tissue-specific expression of candidate CNS-specific genes *BCAN*, *CSPG5*, *PTPRZ1*, *NrCAM*, *CDH10*, *GRM3*, and *MOG* across a subset of tissue samples in GTEx v7. Units shown are normalized RNA-seq counts (transcripts per million) taken from GTEx portal v7. Brain expression is shown in red. See fig. S1 for the pipeline used to identify CNS-specific targets. (**C**) Validation of synNotch receptors that recognize CNS antigens. Receptors (see fig. S2 for more on the generation of receptors) were expressed in primary human $CD4^+$ T cells with a GFP synNotch activation reporter. These cells were cocultured with mouse primary neurons and glia to test activation. Flow cytometry histograms show induction of the GFP reporter only in the presence of primary neuronal and glial cultures. (**D**) Time-lapse images (for full movie, see movie S1) showing primary human $CD8^+$ T cells sensing BCAN expressed by primary astrocytes (red). Primary human $CD8^+$ T cells expressing BCAN-sensing synNotch are shown in blue. The cells turn green when they are activated and induce the GFP reporter. Scale bar, 20 μm. (**E**) The α-BCAN synNotch receptor recognizes extracellular matrix-bound recombinant BCAN. The α-BCAN synNotch receptor was expressed in primary human $CD4^+$ T cells with a GFP synNotch activation reporter. These cells were cultured with mouse or human recombinant BCAN presented on hyaluronic acid–coated plates to test activation. Flow cytometry histograms show the induction of GFP reporters only in the presence of recombinant BCAN.

of chondroitin sulfate proteoglycans, including CSPG5, BCAN, versican (VCAN), and neurocan (NCAN) (Fig. 1, A and B). Many of these proteoglycans are secreted by glial cells such as astrocytes and neuronal cells. This ECM is estimated to account for 20% of the adult brain by volume (*8*), thus potentially providing an ample ligand source for synNotch priming that might be exploited for tissue-specific recognition.

Overall, the 59 putative CNS-specific markers identified in our bioinformatic analysis fell in three broad categories (Fig. 1A): (i) proteins of the CNS-specific ECM, such as BCAN and CSPG5; (ii) proteins on the myelin sheath produced by oligodendrocytes that surround the axons, such as MOG; and (iii) proteins found on neuron surfaces such as CDH10 (brain-specific cadherin) (see fig. S1B for a complete antigen list).

Engineering synNotch sensors for CNS-specific extracellular molecules

To construct brain-sensing cells, we designed and tested synNotch receptors that recognized

our candidate antigens. These synNotch sensors were then used to conditionally induce the transcription of the desired genetically encoded therapeutic payloads. Briefly, synNotch receptors consist of a variable extracellular recognition domain (e.g., a single-chain antibody), a cleavable Notch-based transmembrane domain, and a transcriptional intracellular domain (*4*). Upon antigen binding, the intramembrane receptor is cleaved, releasing the transcriptional domain that can enter the nucleus to activate the expression of a transgene of choice from the synNotch-responsive promoter. Therapeutic payloads can be chosen depending on the nature of the target disease.

We selected seven antigens for use in building cognate synNotch receptors (figs. S1D and S2) including: three CNS ECM proteins, CSPG5, BCAN, and PTPRZ1; three neural surface proteins, CDH10 (cadherin 10), NrCAM (neural cell adhesion molecule), and GRM3 [a metabotropic glutamate receptor (mGluR)]; and one oligodendrocyte surface protein, MOG. We screened a phage antibody library for binding to the human versions of these proteins, and identified one to 10 antibody recognition domains that bound each specific target. MOG binder sequences were identified from the literature. Based on the binding properties of these antibodies, we narrowed down the list to design and build a total of 40 new synNotch receptors using single-chain fragment variables (scFvs) designed from the antibody sequences (40 receptors including the different antigen targets, antibodies, and heavy- and light-chain scFv orientations). We screened these receptors for surface expression and then again for antigen-inducible synNotch activity with low basal background. Because we wanted to evaluate the in vivo targeting function of these receptors in mice, we screened for synNotch receptors that were also cross-reactive against the human and mouse cognate antigen. To functionally test synNotch receptor cross-reactivity, we expressed the receptors in $CD4^+$ T cells with an inducible green fluorescent protein (GFP) reporter. The engineered T cells were cocultured with either primary mouse brain cell cultures or K562 cells (an immortalized chronic myelogenous leukemia cell line) expressing the cognate mouse antigen (fig. S2). Constructs showing antigen-specific induction of GFP without background expression in the absence of antigen were selected for further study. This process resulted in a set of synNotch receptors that could be used to sense six candidate CNS-specific antigens (Fig. 1C).

We were intrigued by the synNotch receptors targeting the ECM because the ECM is abundant and distributed throughout the brain (*8*). BCAN, in particular, is one of the most highly prevalent molecules in the brain ECM. Astrocytes synthesize large amounts of BCAN. Therefore, to test the activity of the α-BCAN synNotch receptor, we cultured primary T cells expressing this receptor with primary mouse astrocytes in vitro. The T cells (blue) contacted the surface of astrocytes (red), and subsequently turned green from activation of the synNotch reporter (Fig. 1D and movie S1). Thus, cultured primary mouse astrocytes produce enough BCAN to drive activation of this synNotch receptor. Reconstituted BCAN-containing hydrogels can also activate cells with the α-BCAN synNotch receptor (Fig. 1E), indicating that this induction can occur in a cell-free manner. Overall, these findings highlight that cells can be engineered to sense specific noncellular microenvironmental features (e.g., the ECM) as a means of recognizing a particular tissue such as the brain.

Using BCAN sensor to anatomically target primary brain tumors in vivo

We explored whether CNS-sensing synNotch receptors could be used to direct CAR T cell killing of brain tumors such as glioblastoma (GBM). As with most solid tumors, there is no perfect single antigen to target on GBM that is both absolutely tumor specific and homogeneously expressed on tumor cells. Nonetheless, there are several glioma-associated antigens, including ephrin type A receptor 2 (EphA2) and the IL-13 receptor α2 (IL13Rα2), that are homogeneously expressed on the surface of most of GBM cells in large amounts (*9*–*11*). However, these antigens are also expressed in normal tissues and are only specific to GBM within the confines of the brain (neither EphA2 nor IL13Rα2 is expressed in nondisease brain cells). Therefore, if T cells could be engineered to only induce the expression of an anti-EphA2 and anti-IL13Rα2 CAR when in the brain, then we could potentially achieve effective GBM killing but also prevent CAR killing of cross-reactive tissues outside of the brain (*12*–*15*). RNA-seq data from the Cancer Genome Atlas Program (TCGA) (*16*) indicated that BCAN is the most strongly expressed of our brain-specific antigens within GBM tumor samples. We thus evaluated T cells engineered with a synNotch circuit in which α-BCAN synNotch promoted the expression of a single CAR receptor recognizing either EphA2 or IL13Rα2 (a tandem CAR that kills cells expressing either antigen) (Fig. 2A).

We then tested whether $CD8^+$ T cells engineered with this BCAN-induced CAR circuit could kill the GBM patient-derived xenograft (PDX) tumor cell line GBM6 in vitro. We observed killing of GBM6 cells in vitro, which was further enhanced in the presence of K562 cells engineered to express BCAN (only low levels of GBM6 killing were observed when cocultured with K562 cells not engineered to express BCAN; Fig. 2B). Thus, although GBM6 cells do express some BCAN, the amount is not sufficient for strong synNotch activation. However, synNotch priming by neighboring $BCAN^+$ K562 cells strongly induced CAR expression and the subsequent killing of GBM6 cells (Fig. 2B and fig. S3A) without causing toxicity to the $BCAN^+$ K562 cells (fig. S3B).

We tested this circuit in vivo, in mice bearing GBM xenografts. GBM6 cells were inoculated in the brains of immunodeficient NCG mice, which were then infused intravenously with either T cells bearing the α-BCAN synNotch→α-EphA2-IL13Rα2 CAR circuit or untransduced control T cells (Fig. 2C). All of the mice receiving the untransduced T cells (n = 5) died of tumor progression by day 51 after tumor cell inoculation. All mice treated with the synNotch-CAR T cells showed complete control and long-term remission of the GBM6 tumors (P = 0.018, mixed-effects analysis), as reflected in their significantly increased survival [P = 0.003, log-rank (Mantel-Cox) test]. Additional repeats highlighted the robustness of this circuit (fig. S3C). The BCAN-primed T cells were more effective than similar MOG-primed T cells (*5*), because they cleared GBM6 tumors more rapidly and with near-perfect consistency, suggesting that this brain ECM target is a more prevalent and effective brain-priming antigen.

To determine where these BCAN-primed T cells were active with higher resolution, we performed confocal imaging on mouse brain samples at 10 days after T cell infusion (Fig. 2D and fig. S4). We observed synNotch-primed T cells throughout the brain slices (induced expression of CAR-GFP), but only observed killing or apoptosis (as shown by active caspase 3 staining) within the tumor. Adjacent neurons (stained for NeuN) did not show apoptosis. Thus, these T cells did not kill the normal brain cells but only specifically killed the EphA2/IL13Rα2–expressing tumor cells.

To further investigate whether BCAN synNotch induction was restricted to the brain, we performed flow cytometric analysis of α-BCAN synNotch→α-EphA2-IL13Rα2 CAR T cells isolated from the blood, spleen, and brain of GBM6 tumor-bearing mice at day 6 after T cell injection. Induced CAR expression was higher in T cells harvested from the brain, consistent with brain-restricted synNotch activation (Fig. 2E and fig. S5A). The T cells isolated from the brain also showed induced expression of CD69 and CD103, markers of T cell activation and retention, respectively (fig. S5A). Altogether, these data are consistent with a brain-restricted antitumor response. The brain-only localization of synNotch-activated T cells is consistent with prior studies showing that that synNotch-induced CAR expression decays with a half-life of a few hours upon removal of the priming antigen (*5*).

We observed that α-BCAN synNotch→α-EphA2-IL13Rα2 CAR T cells persisted in the brains for

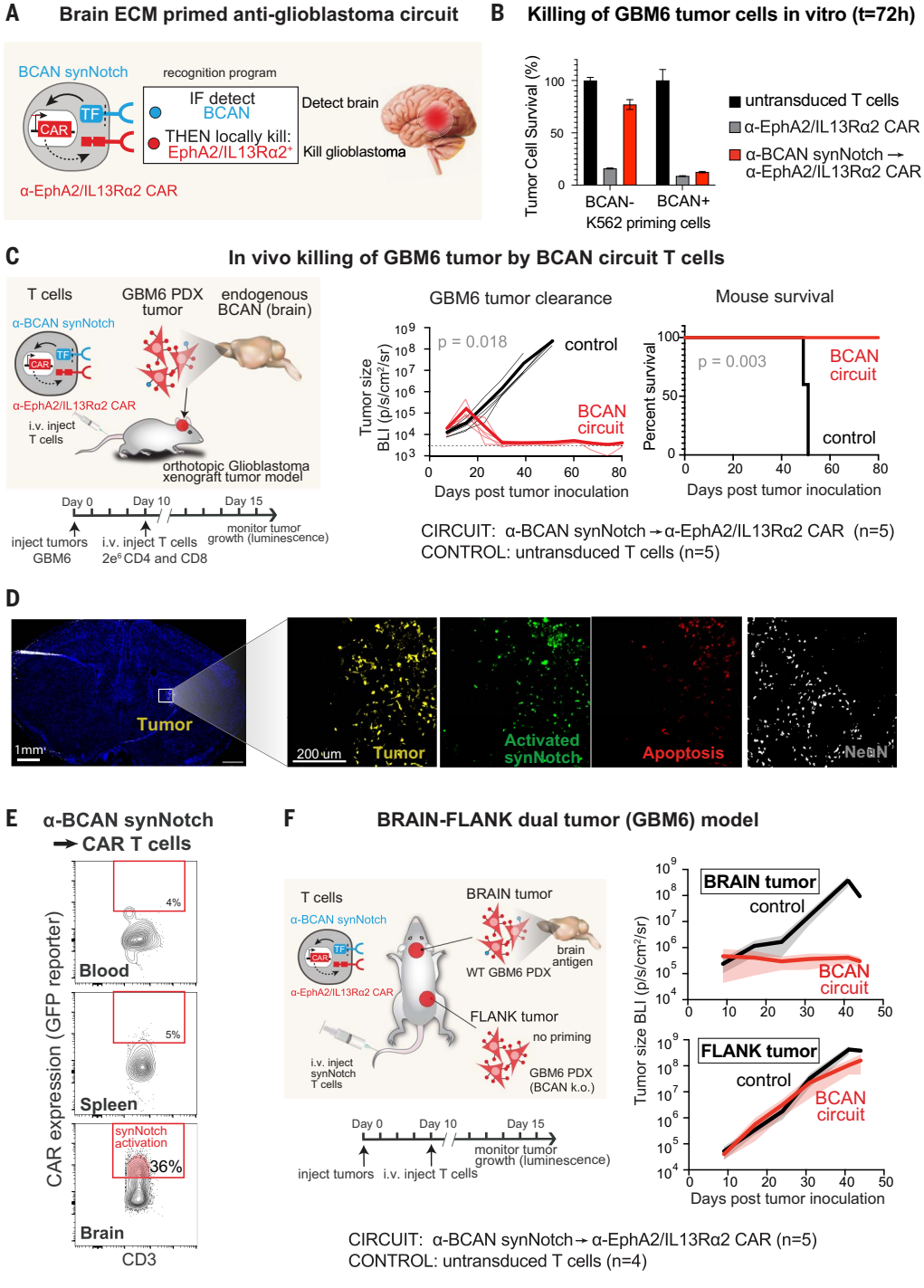

Fig. 2. SynNotch recognition of the CNS-specific ECM molecule BCAN directs CAR antitumor activity specifically and potently to the intracerebral GBM PDX. (**A**) Design of a brain-targeted CAR T cell. The α-BCAN synNotch receptor was used to drive the expression of antitumor CAR only in the brain. This tissue-specific priming circuit was designed to restrict the expression of CAR only to the CNS, preventing damage to normal, non-CNS tissues that express the CAR target antigens EphA2 and IL13Rα2. This circuit should selectively identify GBM cells, which are the only cells expressing EphA2 or IL13Rα2 in the CNS. (**B**) Killing of GBM6 PDX tumors in vitro. Primary CD8$^+$ T cells transduced with the α-BCAN synNotch→α-EphA2/IL13Rα2 CAR circuit (or with the constitutively expressed α-EphA2/IL13Rα2 CAR) were cocultured with GBM6 target cells and K562 priming cells either expressing or not expressing BCAN. Relative cell survival of target GBM6 cells is shown at 72 hours (relative to untransduced T cell controls, n = 3, error bars indicate SEM). See fig. S3, A and B, for further details and controls. (**C**) In vivo clearance of GBM6 tumors. GBM6 tumors expressing mCherry and luciferase were orthotopically inoculated in the brains of NCG mice. Ten days after tumor inoculation, mice were infused intravenously with 2 million each of CD4$^+$ and CD8$^+$ T cells expressing the α-BCAN synNotch→α-EphA2/IL13Rα2 CAR circuit (n = 5) or no construct (negative control) (n = 5). Tumor size and survival were monitored over time by bioluminescence imaging. Thick line shows mean tumor size; thin lines show individual mice. Dotted line shows background bioluminescence. P = 0.018, mixed-effects analysis. Survival was analyzed over 80 days by log-rank (Mantel-Cox) test (P = 0.003). See additional repeats in fig. S3C. BCAN KO GBM6 tumors (fig. S7C) were also cleared with similar efficiency. (**D**) GBM6 tumor–bearing mice were euthanized 10 days after α-BCAN SynNotch→CAR T cell infusion (3 million each of CD4$^+$ and CD8$^+$). Representative confocal fluorescent microscopy of brain sections shows synNotch activation (green) and reveals that T cell–mediated killing (cleaved caspase 3 staining, red stain) is restricted to the tumor (adjacent neurons are not apoptotic, gray NeuN stain). Scale bars, 1 mm (left) and 200 μm (right, enlargement of outlined region). See fig. S4 for further analysis of brain-localized T cells in nontumor regions. (**E**) Flow cytometry of α-BCAN synNotch→α-EphA2/IL13Rα2 CAR T cells isolated from blood, spleen, and brain of a GBM6-bearing mouse at day 6 after T cell injection demonstrating the higher presence of GFP$^+$ primed T cells in the brain compared with the blood or the spleen. See fig. S5 for further analysis of brain-localized T cells. (**F**) Brain-flank dual GBM6 tumor model. GBM6 tumor cells were inoculated in the brains of NCG mice, whereas BCAN KO GBM6 cells were inoculated in the flanks of the identical mice (fig. S7, A and B). Both tumors expressed the CAR-target antigens EphA2 and IL13Rα2, but BCAN was only expressed in the brain. Ten days after tumor inoculation, mice were infused intravenously with 2 million each of CD4$^+$ and CD8$^+$ T cells expressing no construct (control) (n = 4) or α-BCAN synNotch→α-EphA2/IL13Rα2 CAR circuit (n = 5). Tumor size in the brain and in the flank were monitored over time by bioluminescence imaging. Only the tumor inoculated in the brain was reduced over time; the flank tumor grew at the same rate as in the mice treated with nontransduced T cells. Data are representative of two independent experiments. Thick line indicates the mean and shaded area the SEM (see fig. S8 for studies showing efficient in vivo killing of brain-inoculated GBM39 tumors in the PDX line lacking BCAN expression).

weeks to months after tumor regression, consistent with the durable antitumor response (fig. S5B). Flow cytometric analysis of these brain-resident α-BCAN synNotch→α-EphA2-IL13Rα2 CAR T cells isolated from the brain showed increased levels of the homing receptors CXCR3 and CD49d (fig. S5B). To determine whether these persisting α-BCAN synNotch→α-EphA2-IL13Rα2 CAR T cells were still functional in vivo, we rechallenged long-term tumor-cleared mice with GBM6 cells inoculated in the contralateral hemisphere (opposite site of the previously cleared initial tumor). This rechallenge was done 86 days after the first tumor cell inoculation. Three of four mice showed resistance to tumor rechallenge: They did not show detectable tumor growth and survived at least 300 days after initial tumor inoculation (with the one other rechallenged mouse showing slower progression than the control cohort; fig. S5C).

To further examine the underlying mechanisms by which the α-BCAN synNotch→α-EphA2-IL13Rα2 CAR T cells home to and infiltrate the brain tumor, we stained them for adhesion molecules and chemokine receptors (fig. S6). α-BCAN synNotch→α-EphA2-IL13Rα2 CAR T cells expressed the adhesion molecules CD18, CD29, and CD49d, which are required for T cell trafficking to the CNS (*17*), as well as the chemokine receptors CCR2, CCR4, CCR5, CCR6, CCR7, CXCR3, and CXCR4, which have ligands that are up-regulated in patients with GBM (*18*).

To confirm that endogenous brain BCAN is sufficient to induce CAR activity, we used CRISPR-Cas9 to knock out the BCAN gene in the GBM6 tumor cells, which still expressed the CAR target antigens EphA2 and IL13Rα2. We confirmed in vitro that the GBM6 BCAN knockout (KO) cells could only be killed by α-BCAN synNotch→CAR T cells when cultured together with BCAN-expressing K562s cells (but not with parental K562 cells) (fig. S7, A and B). Next, we inoculated the GBM6 BCAN KO cells intracranially in mice, treated them with α-BCAN synNotch→CAR circuit T cells, and monitored tumor size. Even without BCAN expression by the GBM6 cells, the α-BCAN synNotch→CAR circuit T cells could control the tumors in the brain, presumably because of priming by the endogenous brain BCAN (fig. S7C). Because BCAN was not required on the tumor cells, we tested whether other GBM PDX cells lacking BCAN might also be efficiently cleared, making this approach more generalizable. We identified a different GBM PDX line, GBM39, that did not express BCAN, and confirmed that GBM39 cells were not killed by BCAN synNotch→CAR circuit T cells in vitro (fig. S8, A to C). However, the α-BCAN synNotch→CAR circuit T cells efficiently cleared GBM39 tumors inoculated in the mouse brain (fig. S8D). Thus, BCAN in normal brain tissue is sufficient to prime the killing of neighboring tumor cells lacking BCAN expression.

To confirm that induced tumor-killing CAR activity was restricted to the brain, we inoculated GBM6 tumor cells in both the brain and in the flank of the same animal. To eliminate possible priming from BCAN expressed in the GBM6 flank tumors, we used the GBM6 tumor cells lacking BCAN (GBM6 BCAN KO) described above, which cleared when inoculated in the brain (fig. S7C). Thus, the flank-inoculated tumor lacked both intrinsic and environmental BCAN expression but still expressed the target CAR antigens EphA2 and IL13Rα2. We then treated the mice with intravenously infused T cells expressing the α-BCAN synNotch→CAR circuit and monitored the size of both tumors. Only the brain-inoculated tumor was cleared, whereas the flank tumor grew and failed to regress (Fig. 2F). Thus, CAR killing activity was not observed outside of the brain, even for potential target cells expressing the CAR antigens. Antigen-expressing cells outside of the brain were not harmed even while the T cells actively killed the tumors within the brain. This high degree of specific anatomical targeting is consistent with the induced expression of T cell retention molecules (CD69 and CD103), as well as previous measurements showing that synNotch-induced CAR expression rapidly decays with a half-life of hours after the loss of synNotch stimulation (*5*).

Using BCAN synNotch sensor to anatomically target secondary brain tumors

Equipped with a reliable in vivo CNS-sensing synNotch platform, we wanted to test its versatility by expanding its use to other brain tumors such as secondary, metastatic brain tumors. Breast cancer is the most common cancer worldwide (*19*), and a major unmet need is the treatment of the associated secondary lethal brain metastases (extracerebral disease can be controlled in 50% of HER2$^+$ breast cancer patients) (*20*). For HER2$^+$ breast cancers, an α-HER2 CAR is predicted to exhibit toxicity to nontumor cells because HER2 is expressed in several healthy tissues (*15*). However, because HER2 expression is minimal in the normal brain (fig. S9A), we tested whether restricting the killing action of a HER2 CAR to the CNS might allow for effective and safe clearance of breast cancer brain metastases (Fig. 3A). In vitro, CD8$^+$ T cells engineered with the α-BCAN synNotch→α-HER2 CAR circuit effectively killed BT-474 tumor cells, a HER2$^+$ breast cancer model cell line (*21*), but only in the presence of BCAN$^+$ K562 cells to induce priming (BT-474 cells do not to express BCAN) (Fig. 3B).

We inoculated BT-474 HER2$^+$ breast cancer tumors in the brains of NSG mice to emulate metastases (*22*, *23*) and infused the mice with T cells bearing the α-BCAN synNotch→α-HER2 CAR circuit. The BCAN-primed T cells efficiently controlled the BT-474–inoculated brain tumors and increased survival compared with mice treated with untransduced T cells (Fig. 3C).

Using a similar strategy, we examined triple-negative breast cancer (TNBC, meaning the cells do not express estrogen, progesterone, or HER2 receptors), which is associated with an even lower patient survival rate compared with HER2$^+$ tumors (*24*–*26*). The surface antigen trophoblast cell surface antigen 2 (TROP2) is overexpressed in TNBCs and can be effectively targeted with an antibody-drug conjugate therapy (*27*–*30*). TROP2 is also expressed in other nondisease tissues, but its presence in the normal brain is minimal (fig. S9B). Thus, TROP2 could be a good CAR target for brain metastases when combined with brain-restricted induction. CD8$^+$ T cells engineered with the α-BCAN synNotch→α-TROP2 CAR circuit effectively killed BT-20 tumor cells, a TNBC TROP2$^+$ cell line (*31*), in vitro, but only in the presence of BCAN$^+$ K562s to induce priming (BT-20 cells do not express BCAN) (fig. S9C). We inoculated BT-20 tumors in the brains of immunodeficient NSG mice to emulate breast cancer brain metastases and treated them a week later with T cells bearing the α-BCAN synNotch→α-TROP2 CAR circuit. The BCAN-primed T cells efficiently cleared the BT-20 tumors and increased mouse survival relative to control mice treated with untransduced T cells (Fig. 3C).

In summary, the α-BCAN–sensing synNotch circuit induced clearance of breast cancer tumors inoculated within the brain and thus offers a potential strategy to target both HER2$^+$ and TNBC metastases to the brain, which are often far more resistant to standard therapies than the primary tumor. Such a brain metastasis–targeting strategy, however, would need to be used in conjunction with a systemic therapeutic (most of which are less effective against brain metastases).

Engineering brain-targeted immune suppressor cells

Neuroinflammatory diseases such as MS present another difficult therapeutic challenge. We investigated whether it is possible to effectively suppress inflammation in the CNS without causing systemic immune suppression (*32*). Currently approved MS therapies act primarily within the peripheral immune system and are effective for relapsing-remitting MS but not for progressive MS (*33*–*35*). This is thought to be due to compartmentalized inflammation in the form of chronic active lesions that histologically are composed primarily of T cells and activated microglia or macrophages (*36*). Therefore, a major goal in MS is to identify and advance therapeutics that can penetrate the BBB and may promote CNS immune modulation and prevent neurodegeneration, the hallmark feature of progressive MS.

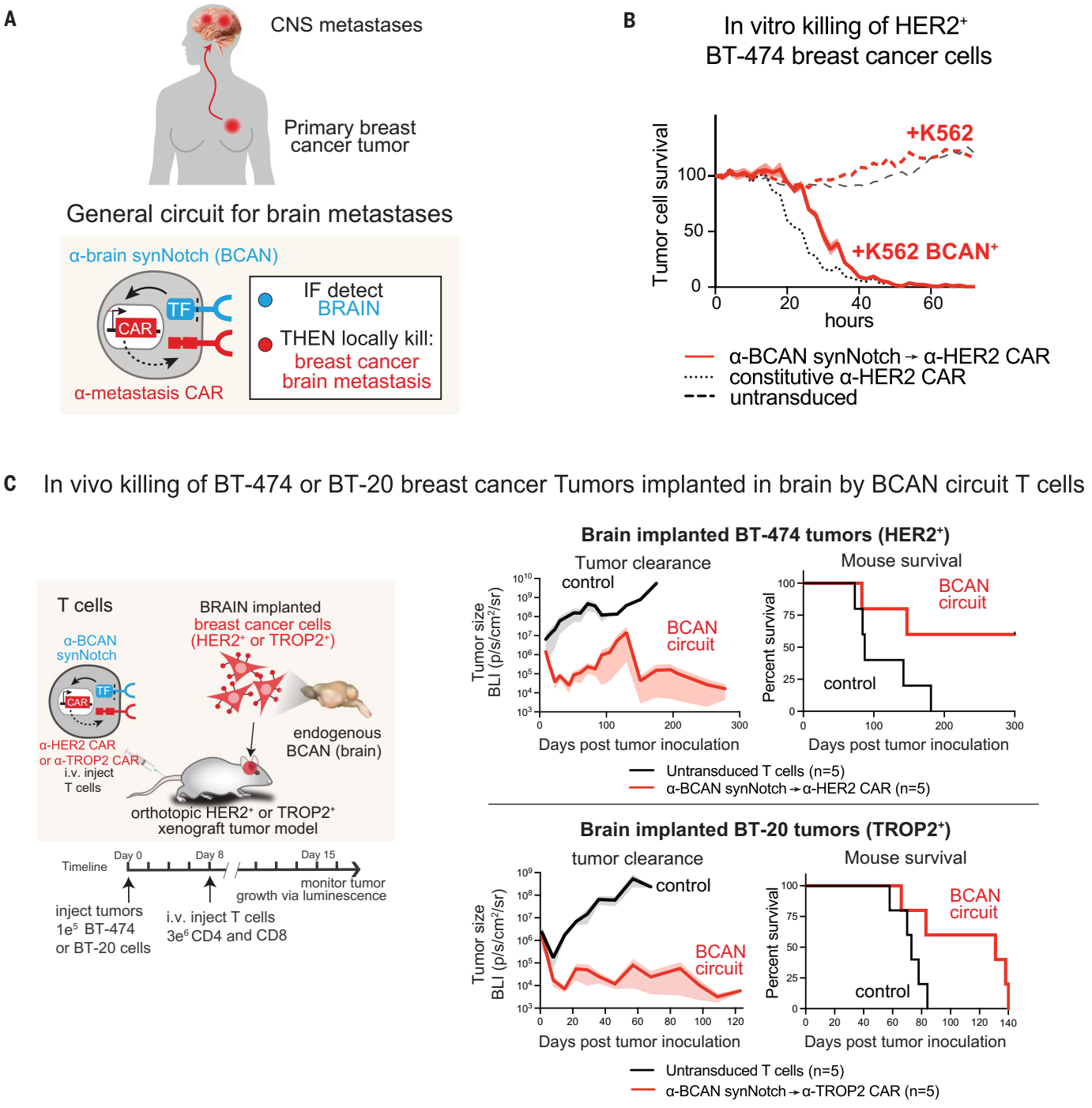

Fig. 3. CNS-specific priming of synNotch-CAR T cells is a generalizable tool for effective killing of brain metastases such as HER2$^+$ and TNBC brain metastases. (**A**) Treatment for CNS metastases is a major unmet need, particularly for breast cancer. A CNS-specific priming circuit could be used as a general platform to target such metastases. Restricting CAR expression only to the brain could prevent damage to normal, nonbrain tissues that express target-killing antigens. Tumor-specific antigens are particularly hard to find for TNBC. Our strategy could be applied to target brain metastases for HER2$^+$ breast cancer or TROP2$^+$ TNBC (fig. S9). (**B**) Real-time in vitro killing of BT-474 breast cancer cells, a model of HER2$^+$ breast cancer. BT-474 cells express HER2 but are negative for BCAN. Therefore, to mimic brain priming, we cocultured BT-474 cells with K562 cells expressing the priming antigen BCAN. Killing of BT-474 cells was only observed in the presence of BCAN$^+$ K562 cells (n = 3, error bars indicate SEM). See fig. S9C for in vitro killing studies of BT-20 breast cancer cells, a model of TNBC. (**C**) In vivo tumor experiments with BT-474 (HER2$^+$ breast cancer) and BT-20 (TNBC) tumors. BT-474 or BT-20 tumors expressing GFP and luciferase were orthotopically inoculated in the brains of NSG mice. Seven days after tumor inoculation, mice were infused intravenously with 3 million each of CD4$^+$ and CD8$^+$ T cells expressing no construct (control) (n = 5) or α-BCAN synNotch→CAR T cells (for BT-474: α-HER2 CAR; for BT-20: α-TROP2 CAR) (n = 5). Tumor size and survival were monitored over time by bioluminescence imaging. Thick line shows mean ± SEM (shaded area).

IL-10, a potent anti-inflammatory cytokine, has been considered an attractive molecule for treatment in both relapsing-remitting and progressive MS. However, intravenous infusion of IL-10 in mouse models and in human clinical trials did not show efficacy (*37*, *38*), likely because of its short half-life (~3 hours in both humans and mice) and its inability to cross the BBB (*39*–*41*). IL-10 might be effective at ameliorating neuroinflammation if it could be effectively delivered to the CNS. Indeed, administration of IL-10 directly in the brain through adenovirus injection successfully ameliorated disease in mouse models of neuroinflammation (*42*). This irreversible viral approach, however, is unlikely to be practical for treatment of MS.

Here, we tested whether brain-sensing T cells could be used as a vehicle to produce IL-10 selectively in the CNS (Fig. 4A). We engineered CD4$^+$ T cells with an α-BCAN synNotch→IL-10 circuit and demonstrated that these cells could effectively produce IL-10 in vitro, but only in the presence of BCAN$^+$ K562 cells (Fig. 4B). To evaluate their anti-inflammatory potential, we tested their ability to inhibit the inflammatory activation of both CNS-autoreactive T cells and microglia cells in vitro. We tested CNS-autoreactive T cells from genetically engineered α-MOG–specific, TCR (2D2) transgenic mice (*43*) (Fig. 4C), and found that their activation [as determined by CD25 staining and interferon-γ (IFN-γ) secretion] was inhibited by α-BCAN synNotch→IL-10 CD4$^+$ T cells in the presence of BCAN$^+$ K562 cells (Fig. 4C). Analogously, we examined mouse microglia cells activated with lipopolysaccharides (LPS) and IFN-γ, as previously described (*44*) (Fig. 4C). In the presence of BCAN$^+$ K562 inducer cells, the α-BCAN synNotch→IL-10 CD4$^+$ T cells reduced secretion of the proinflammatory cytokines IL-6 and TNF-α by activated microglia cells (Fig. 4C). Thus, the α-BCAN synNotch→IL-10 CD4$^+$ T cells can exert immunosuppressive activity against T cells and microglia in vitro.

Brain-targeted suppressor cells ameliorate disease in a mouse model of neuroinflammation

To determine which brain-priming antigens might be best to direct cell therapies against neuroinflammation, we examined published RNA-seq analyses of chronically active MS lesions compared with healthy CNS tissue of patients (*45*). Expression of both BCAN and CDH10 was maintained in MS lesions, but MOG expression was decreased, likely due to demyelination and oligodendrocyte loss in progressive MS (fig. S10). Thus, both BCAN and CDH10 are good candidates for priming brain-targeted responses in neuroinflammatory diseases such as MS. To test the efficacy of these brain-targeted suppressor cells in vivo, we used an established adoptive transfer disease model of EAE (*46*) (Fig. 5A), in which pathogenic polyclonal MOG-autoreactive T helper 17 (T_H17) CD4$^+$ T cells were harvested after direct immunization with MOG peptide into a mouse. These pathogenic cells were adoptively transferred into a recipient immunocompromised RAG-1$^{-/-}$ mouse, inducing severe and usually fatal neurological disease. Using this model, we could test whether infusion of engineered T cells reduced disease severity. Neurological disease severity and progression was tracked with the EAE clinical scoring system, which scores increasing levels of paralysis and neurological dysfunction (*47*–*49*) (Fig. 5A). Adoptive transfer of α-MOG–autoreactive T cells resulted in severe EAE disease in the recipient RAG-1$^{-/-}$ mice, yielding clinical scores close to the maximum of 5 (full paralysis and death). To test our suppressor cells, the mice were injected intravenously every 4 days with the therapeutic synNotch suppressor T cells or control T cells

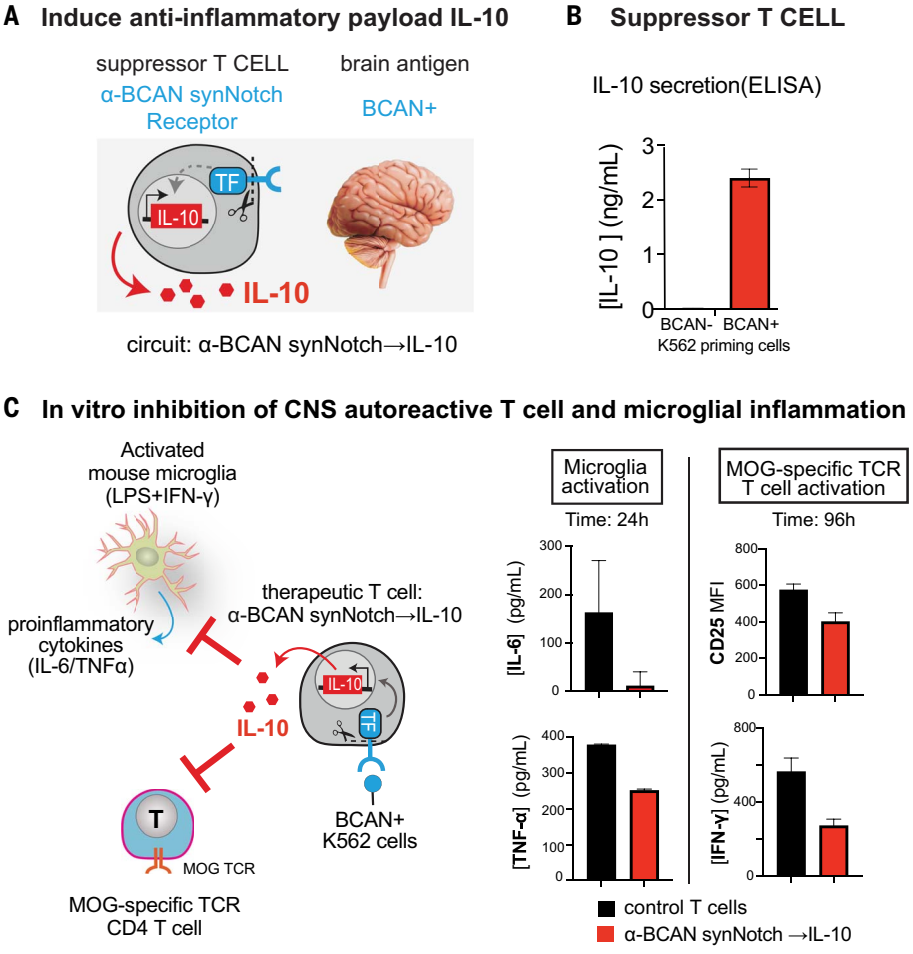

Fig. 4. CNS-specific synNotch circuits can be programmed to produce the anti-inflammatory cytokine IL-10. (**A**) CNS-specific synNotch cells could in principle be used to modulate neuroinflammation. For example, CNS priming could be used to trigger the expression of IL-10, a potent anti-inflammatory cytokine. For more analysis of optimal CNS antigens to target in neuroinflammation, see fig. S10. (**B**) Primary human T cells were engineered with the α-BCAN synNotch→IL-10 circuit and cocultured with K562 cells engineered to express BCAN. Supernatants were collected after 48 hours, and IL-10 was quantified by enzyme-linked immunosorbent assay (ELISA). Quantification shows the specific secretion of IL-10 only when the engineered T cells are cultured with BCAN$^+$ K562 cells (n = 3). (**C**) In vitro inhibition assays of microglia and T cell activation. BV2 mouse microglia were cultured with control or therapeutic T cells (α-BCAN synNotch→IL-10) in the presence of BCAN$^+$ K562 cells to induce payload expression. Two hours later, IFN-γ and LPS were added to induce activation of the microglia. Cells were cultured for 24 hours, and the supernatant was collected to assess inflammation by assaying for secretion of IL-6 and TNF-α by ELISA (n = 3, mean ± SD). Conventional CD25$^-$ TCR$^+$ CD4$^+$ T cells were sorted from MOG-specific TCR (2D2)–transgenic mice and cocultured with antigen-presenting cells presenting MOG peptide to induce their activation. To assay the inhibition of activation, MOG-specific TCR 2D2 CD4 T cells were cocultured at a 1:1 ratio with control transduced or engineered with α-BCAN synNotch→IL-10 T cells for 4 days in the presence of BCAN$^+$ K562 cells to stimulate IL-10 induction. Activation of the MOG-specific TCR 2D2 CD4 T cells was analyzed by flow cytometry using the activation marker CD25 or by ELISA to measure IFN-γ secretion (n = 3, mean ± SD).

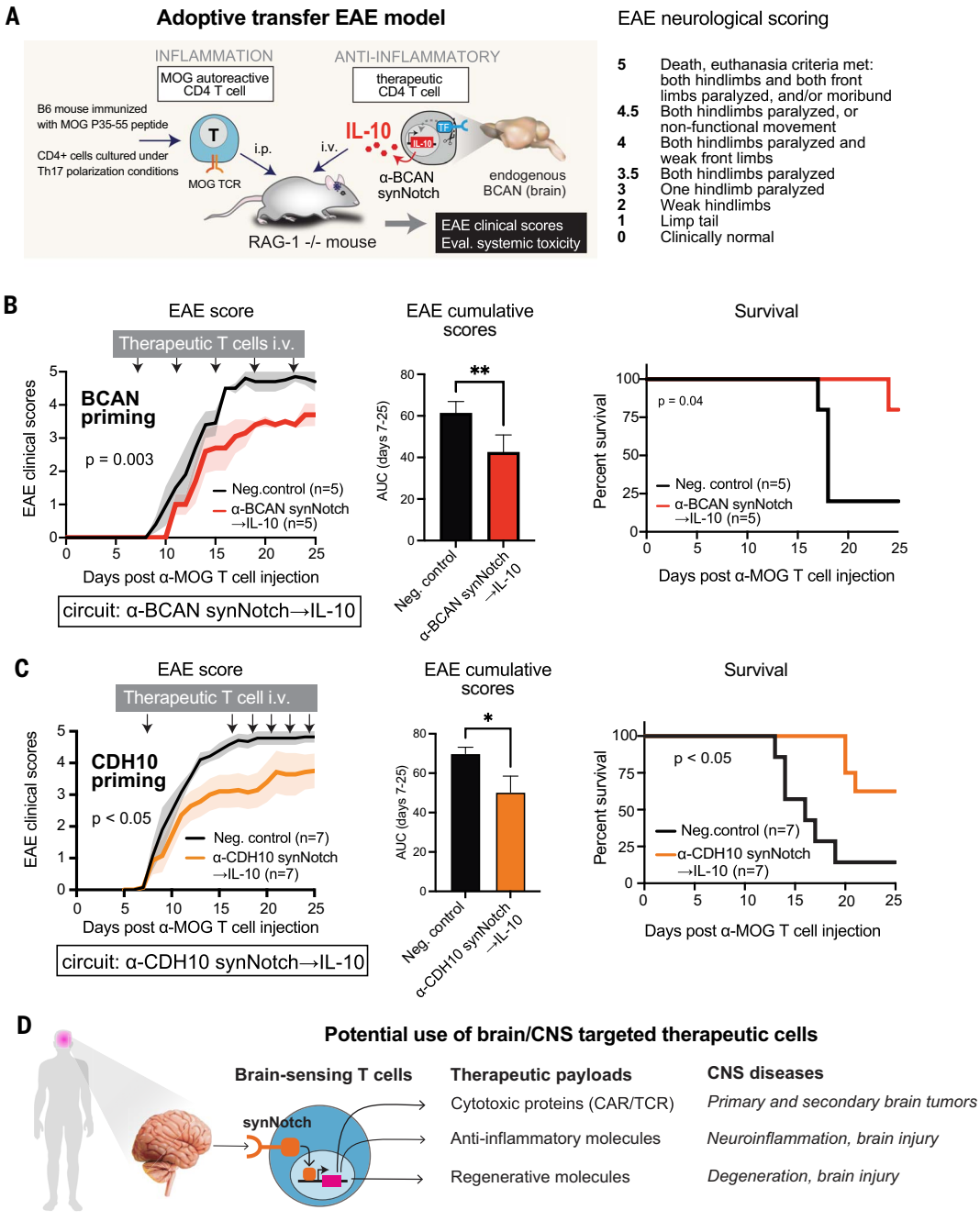

Fig. 5. CNS-targeted anti-inflammatory circuit ameliorates EAE model. (**A**) Schematic of the adoptive transfer EAE model. RAG-1$^{-/-}$ mice received an adoptive transfer of T_H17–polarized CD4 T cells [20 × 10^6 in (B) and 25 × 10^6 in (C)] from P35-55 MOG–immunized C57BL/6J mice. At the indicated days after adoptive transfer (arrows), mice received primary human CD4 T cells transduced with either control (no circuit, n = 5) or α-BCAN synNotch→IL-10 circuit (n = 5) at the indicated times (10 × 10^6). The EAE neurological disease scoring scale is shown. (**B**) Treatment with α-BCAN synNotch→IL-10 T cells yields improved EAE scores and increased survival. Ten million T cells were injected on each day, as indicated by a black arrow. $P < 0.05$, two-way ANOVA. EAE severity was assessed by the area under the curve of each animal starting from the day of first treatment, day 7 until day 25 (n = 5, mean ± SE). $P < 0.05$, unpaired t test. Survival curves show improved protection by the α-BCAN synNotch→IL-10 T cell treatment as analyzed by log-rank (Mantel-Cox) test. The effects of the two treatments on mouse mobility are shown in fig. S11. Additional repeats of this experiment are shown in figs. S12 and S13. (**C**) Treatment with α-CDH10 synNotch→IL-10 T cells yielded improved EAE scores and increased survival. Ten million T cells were injected on each day, indicated by a black arrow. EAE scores showed significant improvements with CNS-targeted α-CDH10 synNotch→IL-10 T cells. $P < 0.05$, two-way ANOVA. EAE severity was assessed by the area under the curve of each animal starting from the day of first treatment, day 7, until day 25 (n = 7, mean ± SE). $P < 0.05$, unpaired t test. Survival curves show improved protection by the α-CDH10 synNotch→IL-10 T cell treatment as analyzed by log-rank (Mantel-Cox) test. (**D**) Brain-sensing cells could be used as a general platform to treat a broad set of CNS diseases such as primary and secondary brain tumors, neuroinflammation, or even neurodegeneration. This customizable platform can be used to locally deliver any genetically encodable molecular therapy that is appropriate for a specific CNS disease, thereby improving on-target action and alleviating off-target toxicity.

expressing blue fluorescent protein (BFP) starting 7 days after the adoptive transfer of the disease-causing α-MOG–autoreactive T cells. The α-BCAN synNotch→IL-10 CD4$^+$ T cells significantly improved disease outcome. We observed less severe EAE scores (P = 0.003, mixed analysis), lowering of cumulative EAE scores, and increased mouse survival relative to mice treated with control T cells (Fig. 5B). Amelioration of EAE disease by the therapeutic cells was supported by the overall increased mobility in the mice treated with α-BCAN synNotch→IL-10 CD4$^+$ T cells (control-treated mice had more severe paralysis; fig. S11). Similarly, treatment with the α-CDH10 synNotch→IL-10 CD4$^+$ T cells also resulted in significantly lower EAE severity scores and improved survival (Fig. 5C). Different dosing regimens of therapeutic T cells provided similar protection (figs. S12 and S13A). Similar to the α-BCAN synNotch→CAR T cells, α-BCAN synNotch→IL-10 CD4$^+$T cells expressed molecules important for trafficking, including the adhesion molecules CD18, CD29, and CD49d and the chemokine receptors CCR2, CCR4, CCR5, CCR6, CCR7, CXCR3, and CXCR4 (fig. S6). Thus, IL-10 produced by brain-sensing T cells (using either BCAN or

CDH10 as a priming antigen) was able to improve symptoms in this EAE model.

To evaluate the importance of brain-primed IL-10 production, we treated EAE mice with analogous suppressor T cells that constitutively express IL-10 (or control T cells constitutively expressing BFP). T cells were injected intravenously every 4 days starting 7 days after adoptive transfer of the disease-causing α-MOG–autoreactive T cells (fig. S13A). Treatment with T cells constitutively expressing IL-10 failed to protect the animals from EAE, consistent with prior reported failure of systemic IL-10 delivery to improve EAE or MS (*37*, *38*). Thus, localized delivery of IL-10 by brain-primed T cells is more effective than constitutive IL-10 production by T cells.

To evaluate whether the α-BCAN synNotch→IL-10 T cells led to any systemic accumulation of IL-10 in the periphery (i.e., outside of the CNS), we measured IL-10 levels in the serum on day 12, after two rounds of therapeutic T cell injections (see fig. S13A). No differences in IL-10 levels were detected compared with negative controls (fig. S13B). However, we observed increased levels of IL-10 in the CNS of mice treated with the α-BCAN synNotch→IL-10 T cells. We also evaluated any signs of systemic IL-10 activity. One of the immunosuppressive mechanisms of IL-10 is to disable antigen presentation and T cell activation through the inhibition of CD80 (B7-1) and CD86 (B7-2) expression on myeloid cells, thereby blocking costimulation (*50*, *51*). Neither group of mice showed a difference in CD80 and CD86 activation markers or PD-1 inhibitory marker expression on the myeloid cells of the spleen, an organ where T cells can accumulate (fig. S13C). Prior studies showed that administration of recombinant IL-10 to healthy patients could result in lower platelet counts in their blood (*39*, *52*), but we observed no differences between the groups (fig. S13D). Thus, IL-10 produced by brain-sensing T cells does not lead to measurable systemic immune suppression or off-target toxicity. These findings validate that brain-sensing cells can serve as a vehicle to deliver anti-inflammatory payloads to the brain with a higher overall therapeutic index.

Discussion

We developed a general cell platform for delivering diverse therapeutic payloads to the brain. We identified several classes of CNS-specific antigens that can be used for CNS targeting of therapeutic cell activity (Fig. 1). These target antigens include components of the specific brain ECM, which offers an abundant and widely distributed targetable substrate because it has a highly distinct molecular composition (*8*). SynNotch receptors that detected the brain ECM component BCAN effectively sensed the native CNS in an in vivo context. Our engineered cells effectively delivered various model payloads directed locally against two distinct types of CNS diseases: cancer and autoimmunity. These observations highlight the broad spectrum of CNS diseases that could potentially be targeted with this approach.

In the case of brain cancer, and cancer in general, it is almost impossible to find a target antigen for CAR T cell therapy that is both homogeneously expressed on all the cancer cells and not expressed in any healthy tissues (*53*–*55*). This explains why the field has had to focus on intracranial T cell injection in the past, with the assumption that the T cells would remain primarily in the brain. As shown here, this conundrum can in some cases be resolved by restricting killing action to a specific anatomical compartment such as the brain. This new strategy is compatible with intravenous delivery of CAR T cells, because the risk of off-target toxicity is limited. In the clinical context, coupling the intravenous route with lymphodepletion will be important to provide more favorable niches for postinfusion expansion, longer-term T cell survival, and potentially a more durable response, as shown for blood cancer CAR T cell treatments. In the intraventricular injection context, CAR T cells have to survive in the cerebrospinal fluid, where the glucose concentration is approximately two-thirds that of the blood and the protein concentration is 100 times lower (*56*). Therefore, this work opens a broad new alternative approach for potentially attacking brain cancers in a safer and more effective way by targeting antigens that are absent in the brain even if they are expressed on healthy tissues elsewhere.

Therapeutic cells that can deliver immunomodulatory cytokines or other biologics to a target tissue such as the CNS can not only make delivery more effective but also reduce the risk of systemic toxicity. Many of these biologics have pleiotropic effects on multiple tissues, which can lead to major toxicities outside of the target tissue. For example, in the case of chronic inflammation, such as MS, systemic treatment with anti-inflammatory drugs can result in an increased risk of infections and other pathologies.

We tested a model anti-inflammatory molecule, IL-10, and validated that its delivery by a brain-sensing T cell improved outcomes in an animal model of neuroinflammation without measurable systemic immune suppression or off-target toxicity. Further, T cells that produced IL-10 in a CNS-induced manner showed greater efficacy than analogous T cells that constitutively produced IL-10. It is noteworthy that persistent inflammation in MS, which is characterized by chronic lesions, ectopic meningeal follicles, and glial activated states, occurs despite current B cell depletion treatments and is a major driver of progressive disability accumulation and atrophy (*57*, *58*). Therefore, localized delivery of IL-10, which can block multiple inflamed cell types (including T cells and microglia) could provide an important additional line of treatment in combination with B cell–depleting therapies. This proof-of-principle study opens the door to a broader examination and screening of diverse cell-delivered anti-inflammatory payloads. It may be possible to develop more effective combinatorial payloads (*59*) or to use further optimized versions of key biologics to further improve therapeutic outcomes (*60*, *61*). The use of allogeneic T cells could help lower the costs of repeated dosing if necessary. Further improving pharmacodynamic and specificity features of the payload cytokine will undoubtedly also lead to more optimized therapies (*39*–*41*).

Nonetheless, future questions remain as to when and how cell-mediated cytokine delivery would ultimately be best deployed for neurological diseases compared with, for example, viral or nonviral vectors with tissue tropism (*62*). Future developments in cell manufacturing and increased cell durability will be critical. Ultimately, however, living cells offer the promise of more sophisticated and controlled cytokine release programs using circuits that spatially and temporally integrate complex environmental cues to achieve more balanced homeostatic control.

Many additional ways could be explored in the future to improve the specificity and efficiency of brain or CNS targeting by therapeutic cells. This could include ways to improve cell trafficking and residence in the brain, as well as to improve cell migration through the BBB. Other important issues to address will be ways to amplify and tune the level of payload production and to increase the durability and survival of the introduced cells.

Overall, our current results suggest that brain-sensing cells could be used as a general platform to treat a broad set of CNS diseases, including brain tumors, brain metastases, neuroinflammation, or even neurodegeneration (Fig. 5D).

The targeting capabilities of engineered immune cells likely exceed the biophysical targeting properties of isolated molecular therapeutics. This approach is inspired by biological specificity, in which many important regulatory molecules are reused throughout the body, but their specific outcomes are restricted by the anatomical locations of the cells that produce them (*63*). In this case, the molecular-scale specificity of the therapeutic payload is layered on top of the anatomical-scale specificity of the cell, yielding much higher combinatorial therapeutic specificity compared with systemic payload administration. Although we focused here on applying this cellular targeting strategy to the brain, this concept could in principle also be applied to target diseases that occur within a broader set of specific tissues. Tissue-targeted

cell delivery provides a general strategy to make therapies more specific and effective and to reduce systemic toxicity.

Materials and methods

Construct design

SynNotch receptors were built by fusing the various scFv sequences (Sidhu lab or patents) to mouse Notch1 (NM_008714) minimal regulatory region (residues 1427 to 1752) and Gal4 DBD VP64. All synNotch receptors contain N-terminal CD8a signal peptide (MALPVTALLLPLALLL HAARP) for membrane targeting and α-myc-tag (EQKLISEEDL) for detecting surface expression with α-myc A647 (Cell Signaling Technology, catalog no. 2233). See Morsut *et al.* (*4*) for the synNotch sequence. Receptors were cloned into a modified pHR'SIN:CSW vector containing a PGK or SFFV promoter. The pHR'SIN:CSW vector was also used to make response element plasmids with five copies of the Gal4 DNA-binding domain target sequence (GGAGCACTGTCCTCCGAACG) upstream from a minimal CMV promoter. Response element plasmids also contain a PGK promoter that constitutively drives BFP expression to easily identify transduced T cells. CARs were built by fusing IL-13 Mutein [E13K,K105R]-G4Sx4-EphA2 scFv (*5*), α-Her2 (4D5) (*21*), or α-TROP2 (hRS7) (*64*) to the hinge region of the human CD8α chain and transmembrane and cytoplasmic regions of the human 4-1BB, and CD3z signaling domains. Inducible CAR constructs or cytokines were cloned into a site 3' to the Gal4 response elements and minimal CMV promoter. CARs were tagged c-terminally with GFP or red fluorescent protein (RFP), or N-terminally with myc tag or flag tag to verify surface expression.

Primary human T cell isolation and culture

Primary $CD4^+$ and $CD8^+$ T cells were isolated from donor blood after apheresis by negative selection (STEMCELL Technologies). Blood was obtained from StemExpress or Allcells, as approved by the University of California San Francisco (UCSF) institutional review board. T cells were cryopreserved either in Cellbanker 1 or in RPMI-1640 with 20% human AB serum (Valley Biomedical) and 10% dimethyl sulfoxide. After thawing, T cells were cultured in human T cell medium consisting of X-VIVO 15 (Lonza), 5% human AB serum, 55 μM β-mercaptoethanol, and 10 mM neutralized *N*-acetyl-L-cysteine supplemented with 30 units/ml IL-2.

Lentiviral transduction of human T cells

Pantropic vesicular stomatitis virus G (VSV-G) pseudotyped lentivirus was produced through transfection of Lenti-X 293T cells (Takara Bio, catalog no. 632180) with a pHR SIN:CSW transgene expression vector and the viral packaging plasmids pCMV and pMD2.G using Fugene HD (Promega) or TransIT-VirusGen (Mirus Bio). Primary T cells were thawed the same day and, after 24 hours in culture, were stimulated with 25 μl of anti-CD3/CD28 coated beads [Dynabeads Human T-Activator CD3/CD28 (Gibco)] per 1×10^6 T cells. In some instances, freshly isolated T cells were used. At 48 hours, viral supernatant was harvested. Primary T cells were exposed to the lentivirus for 24 hours or spinoculated on retronectin-coated plates. At day 5 after T cell stimulation, Dynabeads were removed and T cells were sorted with a BD Biosciences FACSARIA Fusion or Sony SH800S Cell Sorter. T cells exhibiting basal CAR expression were gated out during sorting. T cells were expanded until rested and could be used in assays.

Human T cell staining

T cell expression of adhesion and chemokine receptors were assessed using the following antibodies: APC anti-CD18 (BioLegend, catalog no. 373405), APC anti-CD29 (BioLegend, catalog no. 303007), APC anti-CD49d (BioLegend, catalog no. 304307), APC anti-CD69 (BioLegend, catalog no. 310910), APC anti-CD103e (Invitrogen, catalog no. 2549693), APC anti-LFA-1 (BioLegend, catalog no. 141009), APC anti-CCR1 (BioLegend, catalog no. 362907), APC anti-CCR2 (BioLegend, catalog no. 357207), AF647 anti-CCR3 (BioLegend, catalog no. 310709), AF647 anti-CCR4 (BioLegend, catalog no. 335401), APC anti-CCR5 (BioLegend, catalog no. 359121), APC anti-CCR6 (BioLegend, catalog no. 353415), APC anti-CCR7 (BioLegend, catalog no. 353213), APC anti-CXCR1 (BioLegend, catalog no. 320612), AF647 anti-CXCR2 (BioLegend, catalog no. 320714), APC anti-CXCR3 (BioLegend, catalog no. 353707), APC anti-CXCR4 (BD Biosciences, catalog no. 560936), APC anti-CXCR6 (BioLegend, catalog no. 356005), and corresponding isotype controls. Briefly, post-transfected T cells were sorted, expanded, and rested for ~10 days and then analyzed by flow cytometry. We used a 1:50 antibody dilution. A total volume of 30 μl per staining reaction was used in staining buffer (PBS with 2% fetal bovine serum and 2 mM EDTA). Samples were incubated at 4 °C for 15 min and washed with staining buffer. T cells were analyzed by flow cytometry.

Cell lines

Cell lines used were K562 myelogenous leukemia cells (ATCC catalog no. CCL-243), GBM6, GBM39 PDX cells (gift of Frank Furnari, Ludwig Institute and UCSD), BT-474 (ATCC catalog no. HTB-20) and BT-20 (ATCC catalog no. HTB-19). Cells were lentivirally transduced to stably express GFP or mCherry, and enhanced firefly luciferase under control of the spleen focus-forming virus (SFFV) promoter and sorted as previously shown (*5*). For transgene expression, K562s were transduced with the lentiviral vector CD510-B1 (System Biosciences) and puromycin selected or with pHR based constructs and selected.

GBM6 and GBM39 cells were cultured in DMEM/F12 medium, with supplements of epidermal growth factor (EGF, 20 μg/ml), fibroblast growth factors (FGF, 20 μg/ml), and heparin (5 μg/ml). K562 and BT-20 cells were cultured in DMEM 10% FBS. BT-474 cells were cultured in RPMI with 10% FBS.

In vitro stimulation of synNotch T cells

For in vitro synNotch induction, the engineered T cell and tumor/target cells were cocultured at a 1:1 ratio, with 1×10^5 cells each in a flat-bottomed, 96-well tissue culture plate for 48 hours. When using reconstituted matrix, 2×10^4 cells were cultured for 48 hours on wells coated with hyaluronic acid (200 μg/ml, Thermo Fisher Scientific, catalog no. J60566.MA) and recombinant BCAN (25 μg/ml, R&D Systems, catalog nos. 7188-BC-050 and 4009-BC-050). Cells were analyzed by flow cytometry using a BD Fortessa; analysis was performed with FlowJo software (TreeStar). When cytokine release assays were conducted, the supernatant was collected and processed by ELISA.

In vitro mixed neuronal/glial cultures

Cortexes were dissected from postnatal C57BL/6 (The Jackson Laboratory #000664) day 0 (P0) mice of both sexes, dissociated in 0.25% trypsin, washed three times with Hank's balanced salt solution (HBSS) containing 10 mM HEPES and 20 mM glucose, triturated, and plated on poly-L-lysine–coated coverslips at 350 cells/mm^2. Cells were plated in minimal essential medium containing B27 (Gibco, catalog no. 17504044), 2 mM glutaMAX (Thermo Fisher Scientific, catalog no. 35050061), 5% FBS, 21 mM glucose (Sigma, catalog no. G8769), and 1× penicillin/streptomycin (Thermo Fisher Scientific, catalog no. 15070063). After 1 day in vitro (DIV1), 3/4 of the medium was changed to Neurobasal (Thermo Fisher Scientific, catalog no. 21103049) with B27, glutaMAX, and penicillin/streptomycin.

In vitro astrocyte culture

Astrocytes were isolated from the adult female NCG mouse (Charles River Laboratories) brain tissue using the Adult Brain Disassociation kit (Miltenyi Biotec, catalog no. 130-107-677). Briefly, the extracellular matrix was enzymatically digested along with mechanical dissociation on gentleMACS dissociator with heat. After disassociation, myelin and cell debris were removed using a debris removal solution. The anti–ASCA-2 microbead kit (Miltenyi Biotec, catalog no. 130-097-678) was used to isolate astrocytes from the single-cell suspension. The astrocytes were cultured in a precoated glass-bottomed, six-well plate in AstroMACS medium (Miltenyi Biotec, catalog no. 130-117-031) for 7 days.

Assessment of astrocyte-synNotch CAR T cell interaction

The cultured astrocytes, labeled with MemGlow 590 (20 nM, Cytoskeleton, catalog no. MG03-02), were coincubated with α-BCAN synNotch $CD8^+$ T cells and loaded onto a prewarmed stage (37°C, 5% CO_2) of Zeiss spinning disk confocal microscope. The live-cell imaging (20× magnification) was done for 8 hours with image acquisition at every 5 min.

Assessment of synNotch-CAR T cell cytotoxicity

$CD8^+$ synNotch-CAR T cells were stimulated for up to 72 hours with target cells expressing the killing antigens and, when needed, priming K562 cells (1:1:1, 5×10^4). The degree of specific lysis of target cells was determined by comparing the fraction of target cells alive in the culture with treatment with nontransduced T cell controls unless stated otherwise. Cell death was monitored by shift of target cells out of the side scatter and forward scatter region normally populated by the target cells. Alternatively, cell viability was analyzed using the IncuCyte Zoom system (Essen Bioscience). Tumor cells were plated into a 96-well plate at a density of 2.5×10^4 cells per well in triplicate overnight. Then, 5×10^4 T cells (and K562 cells when specified) were added into each well the next day. Target cells and T cells were cocultured as described above. At least two fields of view were taken per well every 2 to 3 hours. The target cell area was calculated using IncuCyte Zoom software (Essen BioScience) to determine target cell survival. Data were summarized as mean ± SE.

Assessment of autoreactive T cell activation

$CD4^+$ control or synNotch–IL-10 T cells were cultured with K562s expressing BCAN, $CD4^+$, and $CD25^+$ MOG TCR [isolated from C57BL/6-Tg(Tcra2D2,Tcrb2D2)1Kuch/J mice, The Jackson Laboratory #006912], APC [splenic cells that are $CD4^-$, isolated from C57BL/6-Tg(Tcra2D2,Tcrb2D2)1Kuch/J mice, The Jackson Laboratory] in the presence of MOG P35-55 (50μg/ml) at 1:1:1:1 ratio (5×10^4 each) for 4 days. Cells and supernatant were further processed as described in the figures.

Assessment of microglial inflammation inhibition

$CD4^+$ control or synNotch–IL-10 T cells were cultured with K562s expressing BCAN and BV2 microglia cells at 1×10^5, 1×10^5, and 1×10^4, respectively, for 24 hours in medium containing LPS (100 ng/ml) and murine IFN-γ (0.5 ng/ml). Cells and supernatant were further processed as described in the figures.

In vivo mouse experiments

All mouse experiments were conducted according to institutional animal care and use committee (IACUC)–approved protocols. For the orthotopic model with GBM6, and GBM39 5.0×10^4 GBM6-luc-mCherry or GBM39-luc-mCherry cells were inoculated intracranially into 6- to 8-week-old female NCG mice (Charles River Laboratories). For the orthotopic model with BT-474 and BT-20, 1.0×10^5 luc-GFP expressing cells were inoculated intracranially into 8- to 12-week-old female NSG mice (The Jackson Laboratory #005557).

After anesthesia with 1.5% isofluorane, stereotactic surgery for tumor cell inoculation (injection volume: 2 μl) was performed with the coordination of the injection site at 2 mm right and 1 mm anterior to the bregma and 3 mm into the brain. Before and for 3 days after surgery, mice were treated with an analgesic and monitored for adverse symptoms in accordance with the IACUC.

In the subcutaneous model, NCG mice were injected with 1.2×10^5 GBM6-luc-mcherry cells subcutaneously in 100 μl of HBSS on day 0.

Tumor progression was evaluated by luminescence emission on a Xenogen IVIS Spectrum after intraperitoneal injection of 1.5 mg of D-luciferin (GoldBio, injection volume 100 μl). Background bioluminescence was estimated by measuring a nontumor-affected area of the mouse. Before treatment, mice were randomized such that initial tumor burden in control and treatment groups were equivalent. Mice were treated with engineered or nontransduced T cells at indicated doses intravenously through the tail vein in 100 μl of PBS. Survival was evaluated over time until predetermined IACUC-approved endpoint (e.g., hunching, neurological impairments such as circling, ataxia, paralysis, limping, head tilt, balance problems, seizures, and weight loss) was reached.

In the EAE experiments, we used an adoptive transfer model as previously described (46). Briefly, naive 8- to 14-week-old C57BL/6 female mice (The Jackson Laboratory #000664) were injected subcutaneously with 100 μg/mouse of MOG peptide in 0.1 ml of an emulsion of CFA containing 4 mg/ml *Mycobacterium tuberculosis* H37Ra (DIFCO Laboratories) and PBS (1:1). Ten days later, draining lymph nodes and spleens were collected, single-cell suspensions were prepared, and cells were stimulated at 4.5×10^6 cells/ml with 10 μg/ml of MOG P35-55 peptide in the presence of 20 ng/ml recombinant mouse IL-23 (R&D Systems, catalog no. 1887-ML-010) and 10 ng/ml recombinant mouse IL-6 (R&D Systems, catalog no. 406-ML-005). After three days of culture, cells were harvested, washed, and 20 to 25×10^6 cells were injected intraperitoneally into each naive recipient 8- to 14-week-old $RAG1^{-/-}$ mouse (The Jackson Laboratories #002216).

Immunofluorescence

Mice were euthanized before being perfused transcardially with cold PBS. Brains were then removed and fixed overnight in 4% paraformaldehyde–PBS before being transferred to 30% sucrose and were allowed to sink (1 to 2 days). Subsequently, brains were embedded in optimal cutting temperature (OCT) compound (Tissue-Tek; Sakura Finetek, catalog no. 4583). Serial 10-mm coronal sections were then cut on freezing microtome and stored at −80°C. Sections were later thawed, fixed with 10% formalin for 10 min, incubated in blocking buffer (PBS with 5% normal donkey serum) for 40 min, and stained with primary antibodies overnight at 4°C. Primary antibodies used were as follows: CD45 (D9M8I) XP rabbit mAb (Cell Signaling Technologies, catalog no. 1:100), Cleaved Caspase 3 (Asp175) rabbit mAb (Cell Signaling Technologies, catalog no. 1:250), and NeuN mouse mAb (Millipore, clone A60, 1:500).

Conjugated secondary antibodies were used at 4°C for 2 hours to detect primary labeling. Sections were stained with DAPI (Thermo Fisher). Images were acquired using either a Zeiss Axio Imager 2 microscope (20× magnification) with TissueFAXS scanning software (TissueGnostics) or a Stellaris 8 WLL Confocal microscope (20×, 40× magnification) with Leica LAS X imaging software. Exposure times and thresholds were kept consistent across samples within imaging sessions. When needed to improve the visibility of an image, linear adjustment of contrast and brightness was applied to the entire image in accordance with *Science* guidelines (Fig. 2D).

Assessment of engineered T cells in vivo

For all experiments involving phenotyping of adoptively transferred engineered T cells, brain and spleen were harvested after perfusion with cold PBS. Brains were mechanically minced and treated at 37°C for 30 min with a digestion mixture consisting of Collagenase D (30 mg/ml) and DNAse (10 mg/ml) and soybean trypsin inhibitor (20 mg/ml). The resulting brain homogenate was resuspended in 30% Percoll (GE Healthcare), underlaid with 70% Percoll, and then centrifuged for 30 min at 650*g*. Enriched brain-infiltrating T cells were recovered at the 70%–30% interface and stained with fluorescently conjugated antibodies against CD3 (5 μl, BD Biosciences, catalog no. 555342), CD45 (5 μl, BD Biosciences, catalog no. 564357), CD69 (5 μl, BD Biosciences, catalog no. 567066), and CD103 (5 μl, Thermo Fisher Scientific, catalog no. 25-1038-42), CD49d (4 μl, BD Biosciences, catalog no. 563458), CXCR3 (3 μl, BD Biosciences, catalog no. 741005) for 1 hour at 4°C. Before staining with antibodies, cells were stained with BD Horizon Fixability Viability Stain 780 (BD Biosciences) to discriminate live from dead cells. Data were collected on an Attune NxT Flow Cytometer and the analysis was performed in FlowJo software (TreeStar).

Quantification of IL-10 from the serum and CNS homogenates

Blood was collected from intracardial puncture and let to clot at room temperature, followed

by centrifugation to collect the serum. Because in the EAE model, most of the inflammatory demyelinating lesions occur in the spinal cord (*65*), we collected the spinal cord as representative of the CNS in the context of EAE. Mice were perfused with PBS, and the spinal cords were collected and immediately flash frozen in liquid nitrogen. The tissues were then mechanically dissociated in homogenizing buffer [1% Triton X-100, 0.5% NP-40 (tergitol), 25 mM Tris-HCl, pH 7.5, 100 mM NaCl, supplemented with HaltProtease and Phosphatase Inhibitor Cocktail from Thermo Fisher Scientific) using beads and shaking on the Qiagen TissueLyser II. After BCA protein concentration quantification, the samples were resuspended at 2 mg/ml.

The serum was analyzed by Luminex per the manufacturer's instructions after a 1:2 dilution. The tissue homogenates were analyzed with an IL-10 ELISA kit (BioLegend, catalog no. 431414) after a 1:2 dilution.

Assessment of mouse motility

Mice movements were recorded using an iPhone after the experimenter introduced their hand in the cage and either gave a gentle push or moved the mice to the center of the cage. Individual traces of the mice were obtained using the Fiji plugin Manual Tracking for the next 240 frames (8 s). To account for camera movements, the corners of the cage were also tracked, and the mouse displacements were adjusted accordingly.

Statistical analysis

All statistical analyses were performed with Prism software version 9.0 (GraphPad) as described in the figures and legends.

REFERENCES AND NOTES

1. V. L. Feigin *et al*., Global, regional, and national burden of neurological disorders during 1990-2015: A systematic analysis for the Global Burden of Disease Study 2015. *Lancet Neurol.* **16**, 877–897 (2017). doi: 10.1016/S1474-4422(17)30299-5; pmid: 28931491
2. G. C. Terstappen, A. H. Meyer, R. D. Bell, W. Zhang, Strategies for delivering therapeutics across the blood-brain barrier. *Nat. Rev. Drug Discov.* **20**, 362–383 (2021). doi: 10.1038/s41573-021-00139-y; pmid: 33649582
3. J. Smolders *et al*., Tissue-resident memory T cells populate the human brain. *Nat. Commun.* **9**, 4593 (2018). doi: 10.1038/s41467-018-07053-9; pmid: 30389931
4. L. Morsut *et al*., Engineering customized cell sensing and response behaviors using synthetic Notch receptors. *Cell* **164**, 780–791 (2016). doi: 10.1016/j.cell.2016.01.012; pmid: 26830878
5. J. H. Choe *et al*., SynNotch-CAR T cells overcome challenges of specificity, heterogeneity, and persistence in treating glioblastoma. *Sci. Transl. Med.* **13**, eabe7378 (2021). doi: 10.1126/scitranslmed.abe7378; pmid: 33910979
6. R. Dannenfelser *et al*., Discriminatory power of combinatorial antigen recognition in cancer T cell therapies. *Cell Syst.* **11**, 215–228.e5 (2020). doi: 10.1016/j.cels.2020.08.002; pmid: 32916097
7. J. W. Fawcett, T. Oohashi, T. Pizzorusso, The roles of perineuronal nets and the perinodal extracellular matrix in neuronal function. *Nat. Rev. Neurosci.* **20**, 451–465 (2019). doi: 10.1038/s41583-019-0196-3; pmid: 31263252
8. C. Nicholson, E. Syková, Extracellular space structure revealed by diffusion analysis. *Trends Neurosci.* **21**, 207–215 (1998). doi: 10.1016/S0166-2236(98)01261-2; pmid: 9610885
9. K. Bielamowicz *et al*., Trivalent CAR T cells overcome interpatient antigenic variability in glioblastoma. *Neuro-oncol.* **20**, 506–518 (2018). doi: 10.1093/neuonc/nox182; pmid: 29016929
10. M. Hegde *et al*., Combinational targeting offsets antigen escape and enhances effector functions of adoptively transferred T cells in glioblastoma. *Mol. Ther.* **21**, 2087–2101 (2013). doi: 10.1038/mt.2013.185; pmid: 23939024
11. J. Wykosky, D. M. Gibo, C. Stanton, W. Debinski, EphA2 as a novel molecular marker and target in glioblastoma multiforme. *Mol. Cancer Res.* **3**, 541–551 (2005). doi: 10.1158/1541-7786.MCR-05-0056; pmid: 16254188
12. L. A. Johnson *et al*., Gene therapy with human and mouse T-cell receptors mediates cancer regression and targets normal tissues expressing cognate antigen. *Blood* **114**, 535–546 (2009). doi: 10.1182/blood-2009-03-211714; pmid: 19451549
13. M. R. Parkhurst *et al*., T cells targeting carcinoembryonic antigen can mediate regression of metastatic colorectal cancer but induce severe transient colitis. *Mol. Ther.* **19**, 620–626 (2011). doi: 10.1038/mt.2010.272; pmid: 21157437
14. R. A. Morgan *et al*., Cancer regression and neurological toxicity following anti-MAGE-A3 TCR gene therapy. *J. Immunother.* **36**, 133–151 (2013). doi: 10.1097/CJI.0b013e3182829903; pmid: 23377668
15. R. A. Morgan *et al*., Case report of a serious adverse event following the administration of T cells transduced with a chimeric antigen receptor recognizing ERBB2. *Mol. Ther.* **18**, 843–851 (2010). doi: 10.1038/mt.2010.24; pmid: 20179677
16. S. E. Syafruddin, W. F. W. M. Nazarie, N. A. Moidu, B. H. Soon, M. A. Mohtar, Integration of RNA-Seq and proteomics data identifies glioblastoma multiforme surfaceome signature. *BMC Cancer* **21**, 850 (2021). doi: 10.1186/s12885-021-08591-0; pmid: 34301218
17. B. Engelhardt, T cell migration into the central nervous system during health and disease: Different molecular keys allow access to different central nervous system compartments. *Clin. Exp. Neuroimmunol.* **1**, 79–93 (2010). doi: 10.1111/j.1759-1961.2010.009.x
18. P. M. Kollis *et al*., Characterising distinct migratory profiles of infiltrating T-cell subsets in human glioblastoma. *Front. Immunol.* **13**, 850226 (2022). doi: 10.3389/fimmu.2022.850226; pmid: 35464424
19. L. Wilkinson, T. Gathani, Understanding breast cancer as a global health concern. *Br. J. Radiol.* **95**, 20211033 (2022). doi: 10.1259/bjr.20211033; pmid: 34905391
20. J. P. Leone, B. A. Leone, Breast cancer brain metastases: The last frontier. *Exp. Hematol. Oncol.* **4**, 33 (2015). doi: 10.1186/s40164-015-0028-8; pmid: 26605131
21. R. A. Hernandez-Lopez *et al*., T cell circuits that sense antigen density with an ultrasensitive threshold. *Science* **371**, 1166–1171 (2021). doi: 10.1126/science.abc1855; pmid: 33632893
22. D. P. Kodack *et al*., Combined targeting of HER2 and VEGFR2 for effective treatment of HER2-amplified breast cancer brain metastases. *Proc. Natl. Acad. Sci. U.S.A.* **109**, E3119–E3127 (2012). doi: 10.1073/pnas.1216078109; pmid: 23071298
23. J. Ni *et al*., Combination inhibition of PI3K and mTORC1 yields durable remissions in mice bearing orthotopic patient-derived xenografts of HER2-positive breast cancer brain metastases. *Nat. Med.* **22**, 723–726 (2016). doi: 10.1038/nm.4120; pmid: 27270588
24. C. Aversa *et al*., Metastatic breast cancer subtypes and central nervous system metastases. *Breast* **23**, 623–628 (2014). doi: 10.1016/j.breast.2014.06.009; pmid: 24993072
25. N. U. Lin *et al*., Sites of distant recurrence and clinical outcomes in patients with metastatic triple-negative breast cancer: High incidence of central nervous system metastases. *Cancer* **113**, 2638–2645 (2008). doi: 10.1002/cncr.23930; pmid: 18833576
26. C. K. Anders *et al*., The prognostic contribution of clinical breast cancer subtype, age, and race among patients with breast cancer brain metastases. *Cancer* **117**, 1602–1611 (2011). doi: 10.1002/cncr.25746; pmid: 21472708
27. W. Zhao *et al*., Trop2 is a potential biomarker for the promotion of EMT in human breast cancer. *Oncol. Rep.* **40**, 759–766 (2018). doi: 10.3892/or.2018.6496; pmid: 29901160
28. A. Shvartsur, B. Bonavida, Trop2 and its overexpression in cancers: Regulation and clinical/therapeutic implications. *Genes Cancer* **6**, 84–105 (2015). doi: 10.18632/genesandcancer.40; pmid: 26000093
29. M. Trerotola *et al*., Upregulation of Trop-2 quantitatively stimulates human cancer growth. *Oncogene* **32**, 222–233 (2013). doi: 10.1038/onc.2012.36; pmid: 22349828
30. E. Makhoul, F. Dadmanesh, High expression of trophoblast cell surface antigen 2 in triple-negative breast cancer identifies a novel therapeutic target. *Am. J. Clin. Pathol.* **152** (Supplement_1), S37 (2019). doi: 10.1093/ajcp/aqz113.001
31. D. Liu *et al*., Trop-2-targeting tetrakis-ranpirnase has potent antitumor activity against triple-negative breast cancer. *Mol. Cancer* **13**, 53 (2014). doi: 10.1186/1476-4598-13-53; pmid: 24606732
32. G. Schett, M. F. Neurath, Resolution of chronic inflammatory disease: Universal and tissue-specific concepts. *Nat. Commun.* **9**, 3261 (2018). doi: 10.1038/s41467-018-05800-6; pmid: 30111884
33. Y. N. Lamb, Ocrelizumab: A review in multiple sclerosis. *Drugs* **82**, 323–334 (2022). doi: 10.1007/s40265-022-01672-9; pmid: 35192158
34. P. Maggi *et al*., B cell depletion therapy does not resolve chronic active multiple sclerosis lesions. *EBioMedicine* **94**, 104701 (2023). doi: 10.1016/j.ebiom.2023.104701; pmid: 37437310
35. X. Montalban *et al*., Ocrelizumab versus placebo in primary progressive multiple sclerosis. *N. Engl. J. Med.* **376**, 209–220 (2017). doi: 10.1056/NEJMoa1606468; pmid: 28002688
36. J. Zhan, M. Kipp, W. Han, H. Kaddatz, Ectopic lymphoid follicles in progressive multiple sclerosis: From patients to animal models. *Immunology* **164**, 450–466 (2021). doi: 10.1111/imm.13395; pmid: 34293193
37. H. Wiendl, O. Neuhaus, L. Kappos, R. Hohlfeld, [Multiple sclerosis. Current review of failed and discontinued clinical trials of drug treatment]. *Nervenarzt* **71**, 597–610 (2000). doi: 10.1007/s001150050636; pmid: 10996910
38. B. Cannella, Y. L. Gao, C. Brosnan, C. S. Raine, IL-10 fails to abrogate experimental autoimmune encephalomyelitis. *J. Neurosci. Res.* **45**, 735–746 (1996). doi: 10.1002/(SICI)1097-4547(19960915)45:6<735::AID-JNR10>3.0.CO;2-V; pmid: 8892085
39. R. D. Huhn *et al*., Pharmacodynamics of subcutaneous recombinant human interleukin-10 in healthy volunteers. *Clin. Pharmacol. Ther.* **62**, 171–180 (1997). doi: 10.1016/S0009-9236(97)90065-5; pmid: 9284853
40. A. J. Kastin, V. Akerstrom, W. Pan, Interleukin-10 as a CNS therapeutic: The obstacle of the blood-brain/blood-spinal cord barrier. *Brain Res. Mol. Brain Res.* **114**, 168–171 (2003). doi: 10.1016/S0169-328X(03)00167-0; pmid: 12829328
41. L. Li, J. F. Elliott, T. R. Mosmann, IL-10 inhibits cytokine production, vascular leakage, and swelling during T helper 1 cell-induced delayed-type hypersensitivity. *J. Immunol.* **153**, 3967–3978 (1994). doi: 10.4049/jimmunol.153.9.3967; pmid: 7930605
42. D. J. Cua, B. Hutchins, D. M. LaFace, S. A. Stohlman, R. L. Coffman, Central nervous system expression of IL-10 inhibits autoimmune encephalomyelitis. *J. Immunol.* **166**, 602–608 (2001). doi: 10.4049/jimmunol.166.1.602; pmid: 11123343
43. E. Bettelli *et al*., Myelin oligodendrocyte glycoprotein-specific T cell receptor transgenic mice develop spontaneous autoimmune optic neuritis. *J. Exp. Med.* **197**, 1073–1081 (2003). doi: 10.1084/jem.20021603; pmid: 12732654
44. N. Gresa-Arribas *et al*., Modelling neuroinflammation in vitro: A tool to test the potential neuroprotective effect of anti-inflammatory agents. *PLOS ONE* **7**, e45227 (2012). doi: 10.1371/journal.pone.0045227; pmid: 23028862
45. M. L. Elkjaer *et al*., Molecular signature of different lesion types in the brain white matter of patients with progressive multiple sclerosis. *Acta Neuropathol. Commun.* **7**, 205 (2019). doi: 10.1186/s40478-019-0855-7; pmid: 31829262
46. S. A. Sagan *et al*., T cell deletional tolerance restricts AQP4 but not MOG CNS autoimmunity. *Proc. Natl. Acad. Sci. U.S.A.* **120**, e2306572120 (2023). doi: 10.1073/pnas.2306572120; pmid: 37463205
47. Y. Sonobe *et al*., Chronological changes of CD4(+) and CD8(+) T cell subsets in the experimental autoimmune encephalomyelitis, a mouse model of multiple sclerosis. *Tohoku J. Exp. Med.* **213**, 329–339 (2007). doi: 10.1620/tjem.213.329; pmid: 18075237
48. P. M. Mathisen, M. Yu, J. M. Johnson, J. A. Drazba, V. K. Tuohy, Treatment of experimental autoimmune encephalomyelitis with genetically modified memory T cells. *J. Exp. Med.* **186**, 159–164 (1997). doi: 10.1084/jem.186.1.159; pmid: 9207010
49. M. K. Shaw *et al*., Local delivery of interleukin 4 by retrovirus-transduced T lymphocytes ameliorates experimental autoimmune encephalomyelitis. *J. Exp. Med.* **185**, 1711–1714 (1997). doi: 10.1084/jem.185.9.1711; pmid: 9151908
50. C. H. Chang, M. Furue, K. Tamaki, B7-1 expression of Langerhans cells is up-regulated by proinflammatory

cytokines, and is down-regulated by interferon-gamma or by interleukin-10. *Eur. J. Immunol.* **25**, 394–398 (1995). doi: 10.1002/eji.1830250213; pmid: 7533084
51. L. Ding, P. S. Linsley, L. Y. Huang, R. N. Germain, E. M. Shevach, IL-10 inhibits macrophage costimulatory activity by selectively inhibiting the up-regulation of B7 expression. *J. Immunol.* **151**, 1224–1234 (1993). doi: 10.4049/jimmunol.151.3.1224; pmid: 7687627
52. J. A. Sosman *et al*., Interleukin 10-induced thrombocytopenia in normal healthy adult volunteers: Evidence for decreased platelet production. *Br. J. Haematol.* **111**, 104–111 (2000). pmid: 11091188
53. A. J. Hou, L. C. Chen, Y. Y. Chen, Navigating CAR-T cells through the solid-tumour microenvironment. *Nat. Rev. Drug Discov.* **20**, 531–550 (2021). doi: 10.1038/s41573-021-00189-2; pmid: 33972771
54. W. A. Lim, C. H. June, The Principles of Engineering Immune Cells to Treat Cancer. *Cell* **168**, 724–740 (2017). doi: 10.1016/j.cell.2017.01.016; pmid: 28187291
55. D. J. Irvine, M. V. Maus, D. J. Mooney, W. W. Wong, The future of engineered immune cell therapies. *Science* **378**, 853–858 (2022). doi: 10.1126/science.abq6990; pmid: 36423279
56. S. B. Hladky, M. A. Barrand, Mechanisms of fluid movement into, through and out of the brain: Evaluation of the evidence. *Fluids Barriers CNS* **11**, 26 (2014). doi: 10.1186/2045-8118-11-26; pmid: 25678956
57. B. A. C. Cree *et al*., Silent progression in disease activity-free relapsing multiple sclerosis. *Ann. Neurol.* **85**, 653–666 (2019). doi: 10.1002/ana.25463; pmid: 30851128
58. G. Giovannoni *et al*., Smouldering multiple sclerosis: The 'real MS'. *Ther. Adv. Neurol. Disord.* **15**, 17562864211066751 (2022). doi: 10.1177/17562864211066751; pmid: 35096143
59. N. R. Reddy *et al*., Engineering synthetic suppressor T cells that execute locally targeted immunoprotective programs. *Science* **386**, eadl4793 (2024). doi: 10.1126/science.adl4793
60. A. M. Levin *et al*., Exploiting a natural conformational switch to engineer an interleukin-2 'superkine'. *Nature* **484**, 529–533 (2012). doi: 10.1038/nature10975; pmid: 22446627
61. R. A. Saxton *et al*., Structure-based decoupling of the pro- and anti-inflammatory functions of interleukin-10. *Science* **371**, eabc8433 (2021). doi: 10.1126/science.abc8433; pmid: 33737461
62. D. M. Dogbey *et al*., Technological advances in the use of viral and non-viral vectors for delivering genetic and non-genetic cargos for cancer therapy. *Drug Deliv. Transl. Res.* **13**, 2719–2738 (2023). doi: 10.1007/s13346-023-01362-3; pmid: 37301780
63. W. A. Lim, The emerging era of cell engineering: Harnessing the modularity of cells to program complex biological function. *Science* **378**, 848–852 (2022). doi: 10.1126/science.add9665; pmid: 36423287
64. A. Bardia *et al*., Sacituzumab Govitecan-hziy in refractory metastatic triple-negative breast cancer. *N. Engl. J. Med.* **380**, 741–751 (2019). doi: 10.1056/NEJMoa1814213; pmid: 30786188
65. H. Lassmann, M. Bradl, Multiple sclerosis: Experimental models and reality. *Acta Neuropathol.* **133**, 223–244 (2017). doi: 10.1007/s00401-016-1631-4; pmid: 27766432

ACKNOWLEDGMENTS

We thank N. Blizzard, R. Almeida, M. Broeker, P. Lopez Pazmino, S. Sidhu, J. Garbarino, and members of the W.A.L., S.S.Z. and H.O. laboratories for assistance, advice, and helpful discussions. We thank the UCSF Flow Cytometry Core and Microscopy Core. **Funding:** This work was supported by the Weill Institute for Neurosciences, the National Cancer Institute (NCI) of the National Institutes of Health (NIH grant U54CA244438 to W.A.L.); the National Institute of Neurological Disorders and Stroke of the NIH (NINDS grant R35NS105068 to H.O.); the National Cancer Institute (grant P50CA097257 to H.O.); the Sandler Foundation Glioma Precision Medicine Program (H.O. and W.A.L.); the Emerson Collective Cancer Research Fund (W.A.L.); the Mary Jane and Carl Panattoni Charitable Foundation (H.O.); the Parker Institute for Cancer Immunotherapy (H.O.); the Marcus Program (Transformative Integrated Research Award to W.A.L.); the Advanced Research Projects Agency for Health (ARPA-H contract D24AC00084-00 to W.A.L.); the National Multiple Sclerosis Society (grant FG-1907-34738 to M.S.S.); the UCSF Living Therapeutics Initiative (W.A.L.); the Valhalla Foundation (W.A.L.); the UCSF Cell Design Institute (W.A.L.); and the UCSF Helen Diller Family Comprehensive Cancer Center (HDFCCC) Laboratory for Cell Analysis Shared Resource Facility (supported by NIH NCI award P30CA082103). The content is solely the responsibility of the authors and does not necessarily represent the official views of the NIH. **Author contributions:** Conceptualization: M.S.S., P.B.W., S.G., S.S.Z., H.O., W.A.L.; Funding acquisition: M.S.S., S.G., M.R.W., S.S.Z., H.O., W.A.L.; Investigation: M.S.S., P.B.W., S.G., Y.W., S.A.S., J.D., C.S., D. D., P.P-C., J.H., R.Z., B.N., W.Y., Y.T., L.C., N.R.R., O.T., S.H., M.R.W., S.S.Z., H.O., W.A.L.; Methodology: M.S.S., P.B.W., S.G., S.S.Z., H.O., W.A.L.; Project administration: M.S.S., S.G., M.R.W., S.S.Z., H.O., W.A.L.; Supervision: M.R.W., S.S.Z., H.O., W.A.L.; Visualization: M.S.S., P.B.W., Y. W., H.O., W.A.L.; Writing – original draft: M.S.S., P.BW., H.O., W.A.L.; Writing – review & editing: M.S.S., P.B.W., S.G., Y.W., M.R.W., S.S.Z., H.O., W.A.L. **Competing interests:** Several patents have been filed related to this work. These include, but are not limited to, US APP # 63/464,497, 17/042,032, 17/040,476, 17/069,717, 15/831,194, 15/829,370, 15/583,658, 15/096,971, and 15/543,220. W.A.L. is shareholder of Gilead Sciences, Allogene, and Intellia Therapeutics, and previously consulted for Cell Design Labs, Gilead, Allogene, and SciFi Foods. H.O. is on the on the scientific advisory boards for Neuvogen and Eureka Therapeutics. S.L.H. currently serves on the scientific advisory boards of Accure, Alector, and Annexon; has previously consulted for BD, Moderna, NGM Bio, and Pheno Therapeutics; and previously served on the board of directors of Neurona. S.L.H. has received travel reimbursement and writing support from F. Hoffmann-La Roche and Novartis AG for anti-CD20 therapy–related meetings and presentations. The remaining authors declare no competing interests. **Data and materials availability:** All data are available in the main manuscript or supplementary materials. Reagents are available from the corresponding author upon reasonable request. Plasmids from this paper will be made available on Addgene.
 This research was funded in whole or in part by NIH/NCI grant U54CA244438 through the Cancer Moonshot initiative. The author will make the Author Accepted Manuscript (AAM) version available under a CC BY public copyright license.

SUPPLEMENTARY MATERIALS

science.org/doi/10.1126/science.adl4237
Figs. S1 to S13
Movie S1

Submitted 20 October 2023; accepted 23 September 2024
10.1126/science.adl4237